

OPTICAL STUDIES OF 15 HARD X-RAY SELECTED CATAclySMIC BINARIES

JULES P. HALPERN,¹ JOHN R. THORSTENSEN,² PATRICIA CHO,¹ GABRIEL COLLVER,¹
MOKHINE MOTSOLEDI,³ HANNES BREYTENBACH,^{3,4} DAVID A. H. BUCKLEY,⁴ AND
PATRICK A. WOUDT³

¹*Department of Astronomy, Columbia University, 550 West 120th Street, New York, NY 10027, USA*

²*Department of Physics and Astronomy, Dartmouth College, Hanover NH 03755, USA*

³*Department of Astronomy, University of Cape Town, Private Bag X3, Rondebosch 7701, South Africa*

⁴*South African Astronomical Observatory, PO Box 9, Observatory 7935, Cape Town, South Africa*

ABSTRACT

We conducted time-resolved optical spectroscopy and/or time-series photometry of 15 cataclysmic binaries that were discovered in hard X-ray surveys by the *Swift* Burst Alert Telescope (BAT) and the *International Gamma-Ray Astrophysics Laboratory* (*INTEGRAL*), with the goal of measuring their orbital periods and searching for spin periods. Four of the objects in this study are new optical identifications: Swift J0535.2+2830, Swift J2006.4+3645, IGR J21095+4322, and Swift J2116.5+5336. Coherent pulsations are detected from three objects for the first time, Swift J0535.2+2830 (1523 s), 2PBC J1911.4+1412 (747 s), and 1SWXRT J230642.7+550817 (464 s), indicating that they are intermediate polars (IPs). We find two new eclipsing systems in time-series photometry: 2PBC J0658.0–1746, a polar with a period of 2.38 hr, and Swift J2116.5+5336, a disk system that has an eclipse period of 6.56 hr. Exact or approximate spectroscopic orbital periods are found for six additional targets. Of note is the long 4.637-day orbit for Swift J0623.9–0939, which is revealed by the radial velocities of the photospheric absorption lines of the secondary star. We also discover a 12.76 hr orbital period for RX J2015.6+3711, which confirms that the previously detected 2.00 hr X-ray period from this star is the spin period of an IP, as inferred by Coti Zelati et al. These results support the conclusion that hard X-ray selection favors magnetic CVs, with IPs outnumbering polars.

Keywords: novae, cataclysmic variables — X-rays: binaries

1. INTRODUCTION

Cataclysmic variables (CVs) are accreting binaries in which a dwarf star donates mass to a white dwarf (WD) via Roche-lobe overflow. This paper is the third in a series presenting detailed studies of new CVs that were discovered in surveys at hard X-rays energies (> 15 keV) by the *Swift* Burst Alert Telescope (BAT) and the *International Gamma-Ray Astrophysics Laboratory* (*INTEGRAL*/IBIS). We measure the CVs' orbital periods using time-resolved optical spectroscopy and/or time-series photometry, while the fast photometry also reveals spin modulation when present, allowing for classification of magnetic subclasses of CVs.

Systems in which the magnetic field of the WD is strong enough to truncate the accretion disk at a magnetospheric boundary, or prevent a disk from forming at all, are particularly efficient at producing hard X-rays. In such systems, an accretion column is channeled onto the magnetic pole or poles, where thermal bremsstrahlung X-rays are emitted by shock-heated plasma just above the surface of the WD.

When the WD magnetic field is strong enough to channel the accreting matter in a stream all the way from the companion, the WD rotation is usually locked to the binary orbit. These systems are the polars (or AM Herculis stars). Polars are also circularly polarized in the optical, and have optical/IR humps in their spectra; both these features are from cyclotron radiation in the strong magnetic field. There are also a few asynchronous polars, in which the spin and orbit periods can differ by as much as a few percent (e.g., [Halpern et al. 2017](#); [Tovmassian et al. 2017](#)).

Intermediate polars (IPs, or DQ Herculis stars) have weaker magnetic fields, which allow the formation of an accretion disk, but a truncated one in which an accretion stream or curtain is channeled from the inner edge of the disk at the magnetosphere boundary to the magnetic pole(s). The spin period of the WD in an IP can be detected as a coherent X-ray or optical oscillation arising from the rotating hot spot at the base of the accretion column, at a shorter period than the orbital period of the binary. Sometimes the beat period between the spin and orbit periods is seen due to reprocessed emission.

Prior to our work, the *Swift*-BAT 70-month hard X-ray survey ([Baumgartner et al. 2013](#)) included 55 known CVs, of which 41 are magnetic: 31 IPs and 10 polars. It is thought that IPs outnumber polars in hard X-ray samples because of their higher accretion rates, and also because in polars, the accretion may be “blobby,” depositing some fraction of the energy directly onto the surface of the WD; the energy is then radiated at lower temperatures, tens of eV. Our goal is to extend the completeness and classification of hard X-ray selected CVs by studying unidentified sources from *Swift*-BAT and *INTEGRAL*/IBIS. In Thorstensen & Halpern (2013, Paper I) and Halpern & Thorstensen (2015, Paper II) we presented data and findings on 23 hard X-ray selected CVs, 10 of which were unidentified X-ray sources prior to our work.

This paper continues the effort with information on another 12 objects, as well as additional data on three CVs from Paper II. Several of these are located close to the Galactic plane and were classified by [Baumgartner et al. \(2013\)](#) simply as “Galactic” based on their coordinates. Targets were selected using published optical spectral information on identified sources. Unidentified X-ray sources were also chosen if they had counterparts in pointed observations with the imaging *Swift* X-ray Telescope (XRT), and/or a relatively bright or blue stellar optical counterpart in the *Swift* UV/Optical Telescope (UVOT). These criteria were found to be efficient in identifying CVs. As a

result, in this paper, we identify 4 new CV counterparts and characterize 11 that were previously identified spectroscopically but lacked detailed studies in the literature.

2. EQUIPMENT AND TECHNIQUES

Our instrumentation as well as our reduction and analysis procedures are similar to those described in Papers I and II, and they are summarized in this section. Nearly all of our optical data are from the MDM Observatory, which comprises the 1.3 m McGraw-Hill telescope and the 2.4 m Hiltner telescope, both on the southwest ridge of Kitt Peak, Arizona. The spectroscopy and radial velocity studies to search for the orbital periods were done mostly on the 2.4 m, while high-cadence photometry sensitive to spin periods was carried out on both of these telescopes, or, for two southern targets, at the South African Astronomical Observatory (SAAO).

2.1. Spectroscopy

Most of our radial velocity studies used the modular spectrograph (modspec) on either the 2.4 m or 1.3 m telescope. In addition to wavelength calibrations using comparison lamps of Hg, Ne, and Xe taken during twilight, we used the night-sky O I $\lambda 5577$ line to track and correct for spectrograph flexure during the night. The projected slit width was $1''$ on the 2.4 m, and $\sim 1''.8$ on the 1.3 m. At the 2.4 m, we rotated the instrument to orient the slit close to the parallactic angle when at large hour angles and zenith distances. The amount of light lost to occasional clouds and at the narrow slit cannot be estimated reliably, but experience suggests that the flux calibration of our averaged spectra is typically accurate to $\sim 20\%$. For unknown reasons, spectra taken with modspec sometimes show irreproducible distortions in their continua, which at least tend to average out; the spectra also are vignettted toward the ends of the 4210–7500 Å spectral range.

We also obtained some spectra using the Ohio State Multi-Object Spectrograph (OSMOS; [Martini et al. 2011](#)) on the 2.4 m. For these, we used the $1''.2$ “inner” slit and a volume-phase holographic grism, which gave coverage from 3980 to 6860 Å at $0.72 \text{ Å pixel}^{-1}$, with a FWHM resolution near 4 Å.

We reduced our spectra using Pyraf scripts that for the most part called IRAF¹ tasks. To extract one-dimensional spectra, we implemented the algorithm published by [Horne \(1986\)](#). We measured emission-line radial velocities using convolution algorithms described by [Schneider & Young \(1980\)](#) and [Shafter \(1983\)](#). To measure synthetic magnitudes from our spectra, we used the [Bessell \(1990\)](#) tabulation of the V passband and the IRAF `sbands` task.

To search for periods in the spectroscopic time series, we used a “residual-gram” algorithm ([Thorstensen et al. 1996](#)). Observing constraints sometimes led to ambiguities in the daily cycle count. To assess the reliability of the cycle count, we used the Monte Carlo methods of [Thorstensen & Freed \(1985\)](#).

For three newly identified objects, we have only single spectra that were obtained on two observing runs on the 2.4 m, using either modspec or OSMOS. Further details on these instruments can be found on the MDM Observatory web page.²

2.2. Time-series Photometry

¹ IRAF is distributed by the National Optical Astronomy Observatory, which is operated by the Association of Universities for Research in Astronomy (AURA) under cooperative agreement with the National Science Foundation.

² <http://mdm.kpno.noao.edu/index/Instrumentation.html>

For most of our time-series photometry, we used “Templeton,” a thinned, back-illuminated SITe CCD with 1024×1024 $24\ \mu$ pixels, each subtending $0.''508$ at the 1.3-m. To minimize read time, the CCD was windowed to 256×256 pixels. Integration times ranged from 20 to 90 s, with 3 s dead-time between exposures. A couple of time series were obtained on the 2.4 m using OSMOS in imaging mode. Some of our data are from a thermoelectrically cooled Andor Ikon DU-937N CCD camera as described in Paper I. Its frame-transfer CCD has a dead-time of only 11.92 ms. Exposure times with the Andor ranged from 15 to 60 s. Filters used were *V* or *R* for bright stars or, more commonly, a broadband Schott GG420 to maximize throughput for fainter stars. GG420 is a long-pass filter transmitting $\lambda > 4200\ \text{\AA}$ that is also useful for suppressing scattered moonlight.

For our SAAO time-series photometry, we mainly used the Sutherland High-Speed Optical Camera (Coppejans et al. 2013) on the 1 m telescope. A small amount of data is from an identical camera on the 1.9 m Radcliffe telescope, and part of a single night was from the SAAO CCD camera mounted on the 1 m. Filters were not used at SAAO.

Differential photometry with respect to a single comparison star that was typically 2–4 mag brighter than the variable was performed using the IRAF task `phot`. Sequences on individual stars ranged from 1.5 to 9.5 hr. Approximate magnitudes were derived for the *V* filter by averaging the *B* and *R* magnitudes of the comparison star in the USNO B1.0 catalog (Monet et al. 2003), or adopting the *R* magnitude of the comparison star for the GG420 filter. Period searches used the Lomb–Scargle periodogram (Scargle 1982), after converting the mid-times of the exposures to barycentric dynamical time (TDB) using the utility of Eastman et al. (2010).

3. RESULTS ON INDIVIDUAL OBJECTS

The objects observed are listed in Table 1, which provides accurate celestial coordinates, approximate magnitudes, and periods where determined. Figure 1 presents finding charts for nine optical counterparts that have not appeared in the literature before, and Figure 2 shows spectra of three of the newly identified stars. Concerning the radial velocity studies, Table 2 lists the velocity data and Table 3 gives parameters of the best-fit sinusoids. Figures 3 and 4 show mean spectra, radial velocity periodograms, and folded radial velocities for six of the objects. The time-series photometry appears in subsequent figures. Table 4 gives eclipse timings.

3.1. *Swift* J0535.2+2830

Baumgartner et al. (2013) identified the brightest XRT source in this field as the counterpart of this BAT source in the Galactic plane. On 2015 November 7 we obtained a spectrum with modspec of the optical object nearest to the XRT position, identified in Figure 1, which shows Balmer emission lines and He II $\lambda 4686$ (Figure 2), typical of a magnetic CV. Time-series photometry in 2016 December with Templeton and in 2017 January with Andor (Figure 5) revealed a single period, refined to 1523.07 ± 0.09 s after connecting the nights in phase. *Swift* J0535.2+2830 is thus a new IP. We do not yet have time-resolved spectroscopy to search for its orbital period.

3.2. *Swift* J0623.9–0939

In Paper II we identified this source from Baumgartner et al. (2013) as the the brightest one in XRT images of the field. It corresponds to 1RXS J062406.9–093815. Only one optical spectrum, having emission lines typical of a CV, had been obtained, as well as one 5.3 hr time series that shows flickering but no obvious period.

We have since obtained further time-resolved spectroscopy (Figure 3) which, in addition to the emission lines, shows an absorption-line component with a radial velocity period of 4.637 ± 0.008 days. This is unusually long for a CV; of the 1429 objects listed by Ritter & Kolb (2016) in their final edition (version 7.24), only one has a longer period, V1017 Sgr at $P_{\text{orb}} = 5.714$ days; the next longest, MR Vel, is at 4.029 days. Even so, the long period fits the absorption velocities much better than any shorter period, and we are confident that the cycle count is correct.

Interestingly, the binary evolution calculations of Kalomeni et al. (2016) predict a population of CV-like systems with periods in the range 2–40 d and secondary stars in the $0.3\text{--}0.8 M_{\odot}$ range; this may be a rare example of such a system.

We estimate that the secondary’s spectral type is between K0 and K5, with the best match toward the warmer part of the range. This constrains the secondary’s surface brightness. The secondary must also fill its Roche lobe, the radius of which depends on P_{orb} , and (more weakly) on M_2 , the mass of the secondary. The surface brightness and radius R_2 yield an absolute magnitude M , which, combined with the secondary’s observed flux, yields a distance, after correction for reddening. We used a Monte Carlo technique described in Paper I to compute a range of distances, sampling each input value from a plausible range. We used the three-dimensional dust maps of Green et al. (2015)³ to improve upon our earlier practice, which had been to treat the extinction as an independent random variable. Instead, we converted distance moduli ($m - M$) to physical distance using the extinction appropriate to each modulus. Guided by the evolutionary calculations of Kalomeni et al. (2016), we drew M_2 from uniform distribution from 0.3 to $0.8 M_{\odot}$. The result was a median distance of 1900 ± 400 pc, where the uncertainty is one standard deviation.

3.3. *2PBC J0658.0–1746*

This X-ray source is listed in the second Palermo *Swift*-BAT hard X-ray catalog (Cusumano et al. 2010), and corresponds to 1RXS J065806.3–174427. It was identified spectroscopically by Rojas et al. (2017), who suggested that it is a magnetic CV, likely an IP, based on its ratio of He II $\lambda 4686/H\beta > 0.5$. We found that the optical position of the star listed in Rojas et al. (2017) is off by $8''$ in decl.; see Table 1 for the correct position and see Figure 1 for a finding chart of this crowded field. Altmann et al. (2017) list a significant proper motion of $(-31.8, +35.9)$ mas yr⁻¹.

We obtained time-series photometry on three nights in 2017 December (Figure 6), the first night using OSMOS on the 2.4 m with an *R* filter, and subsequently using Templeton with a GG420 filter on the 1.3 m. A fourth time-series was obtained with Andor on the 1.3 m on 2018 February 24. A strongly modulated light curve with a double peak, as well as a deep dip lasting 10.6 minutes and repeating on a 2.38 hr period, are evident. These properties are typical of an eclipsing polar. See Warren et al. (1995) and Sirk & Howell (1998) for models of similar light curves. The double peak spans 0.66 of the cycle and can be attributed to a single accreting spot that is visible for this fraction of the rotation, while the broad, V-shaped central depression in the peak is due to partial obscuration of the spot by the accretion stream feeding it. The narrow dip is consistent with total eclipse of the WD by the companion. The changing luminosity of the peaks from night to night can be caused by a variable accretion rate, while the flat, interpeak region (from the full WD area) and the eclipse magnitude (when the secondary dominates the light) remain relatively constant.

³ Their estimates of reddening versus distance modulus can be found at <http://argonaut.skymaps.info/query>.

Quantitatively, the approximate relation between orbital period and secondary mass predicts $M_2 \approx 0.24 M_\odot$, while the ratio of the radius of a Roche-lobe-filling secondary to the binary separation is $R_L/a \approx 0.30$ (Knigge 2011). In this case, the maximum possible eclipse duration would be $\Delta\phi \approx 0.098$ cycles, which is consistent with the observed $\Delta\phi = 0.074$ cycles. A main-sequence star of $0.24 M_\odot$ has absolute magnitude $M_V \approx +13$ and $V - R \approx 1.5$ (Benedict et al. 2016). If the observed magnitude in eclipse of $R \approx 18.5$ is due entirely to the secondary star, then its distance is ≈ 250 pc.

We observed a total of six eclipse ingresses and eight egresses. Some of the eclipse data were degraded by detector noise (December 10) and wind shake (December 19). Nevertheless, the transitions, except for the first egress on December 10, can be timed to a fraction of the ≈ 1 minute observing cadence (10 s cadence with Andor). From a linear fit of the cycle count and egress times listed in Table 4, we derive ephemerides (in TDB) of

$$T_{\text{ingress}} = \text{BJD } 2458102.859282(44) + 0.09913385(12) \times E$$

$$T_{\text{egress}} = \text{BJD } 2458102.866589(51) + 0.09913408(21) \times E$$

In order to measure the spin period from the emission peaks, we excised the points during eclipse and calculated the Lomb-Scargle periodogram of the 2017 data. The resulting spin period is 0.09911(5) day, consistent with the eclipse period albeit at a lower level of precision.

3.4. *Swift* J0717.8–2156

Baumgartner et al. (2013) noted that this source in the Galactic plane corresponds to 1RXS J071748.9–215306. We identified the optical counterpart in Paper II using a single optical spectrum, showing that Swift J0717.8–2156 is a likely CV with $H\alpha$ and $H\beta$ emission, as well as faint He I $\lambda 5876$. Rojas et al. (2017) also obtained a spectrum, showing that the ratio of He II $\lambda 4686/H\beta > 0.5$.

We obtained more extensive spectra in 2016 February. The mean spectrum (Figure 3) shows hydrogen Balmer emission along with emission at He I $\lambda\lambda 5876, 6678, \text{ and } 7067$, and He II $\lambda\lambda 4686$ and (weakly) 5411. The radial velocities of $H\alpha$ give an unambiguous period of 5.51 ± 0.03 hr. A few spectra obtained 2014 December appear similar to the 2016 February data, but do little to constrain P_{orb} .

The detection of He II suggests that Swift J0717.8–2156 may be a magnetic system, but we do not have any time-series photometry on it, which would be needed to further characterize its nature.

3.5. *2PBC* J0801.2–4625

This source from the second Palermo *Swift* BAT hard X-ray catalog (Cusumano et al. 2010), was also detected by *INTEGRAL* (Bird et al. 2016) and is identified with 1RXS J080114.6–462324. Masetti et al. (2010) classified it spectroscopically as a CV. Bernardini et al. (2017) reported on an *XMM-Newton* observation that revealed a spin period of 1310.9 ± 1.5 s in X-rays and 1306.3 ± 0.9 s in the Optical Monitor (OM) *V*-band. In 2017 February, we obtained three short time series on 2PBC J0801.2–4625 at SAAO (Figure 7). The spin oscillation is clearly seen in unfiltered light. A coherent power spectrum cannot distinguish among several aliases, as shown in Figure 7, but only one peak, at 1307.55 ± 0.10 s, is consistent with the *XMM-Newton* value. Therefore, we consider this to be the refined spin period.

3.6. *Swift* J0927.7–6945

This source from Cusumano et al. (2010) and Baumgartner et al. (2013) was identified spectroscopically as a magnetic CV by Parisi et al. (2014) based on its strong He II $\lambda 4686$ emission line. An *XMM-Newton* observation by Bernardini et al. (2017) found periods of 1033.54 ± 0.51 s and 1093.4 ± 6.5 s, which they attribute to the spin and beat period, respectively, of an IP, implying an orbital period of 5.25 ± 0.45 hr. Alternatively, a sinusoidal fit to the X-ray light curve gave $P_{\text{orb}} = 5.15 \pm 0.10$ hr. The spin period was also detected in the OM *B*-band, at 1030.6 ± 0.9 s.

We obtained time-series photometry of Swift J0927.7–6945 at SAAO on five consecutive nights in 2015 February (Figure 8). A coherent power spectrum clearly shows the spin period at 1033.05 ± 0.15 s, and another peak at 4.79 hr. The corresponding beat period would be 1099 s, and indeed there is a weaker peak in the power spectrum at 1098.02 ± 0.16 s. This is consistent with the beat period in X-rays, and can be interpreted as evidence that the orbital period is 4.85 ± 0.02 hr, consistent with the one inferred from X-rays. These results are summarized in Table 1.

3.7. 2PBC J1911.4+1412

This X-ray source is listed in the second Palermo *Swift*-BAT hard X-ray catalog (Cusumano et al. 2010), and was identified spectroscopically by Rojas et al. (2017), who suggested that it is a distant low-mass X-ray binary because of the reddening of its spectrum. However, we conjectured that it could just as well be a moderately reddened CV. Rojas et al. (2017) disfavored the latter, apparently because of their assumption that a CV has absolute magnitude $M_V = +9$, which would require 2PBC J1911.4+1412 to be too nearby for its reddening. However, that assumption is too restrictive; $M_V = +9$ is found only in the lowest-luminosity CVs.

We obtained time-series photometry on five nights in 2017 May–June. A GG420 filter was used with either Templeton (30 s exposures) or Andor (15 s exposures). The results in Figure 9 show regular pulsations with full amplitude ranging from 0.5 to 1 mag. It was possible to phase connect the data from all of the nights, yielding a period of 746.885 ± 0.008 s. Clearly, 2PBC J1911.4+1412 is a new IP. There is no evidence of an orbital period in the photometry, and we have no time-resolved spectroscopy to search for one.

3.8. *Swift* J2006.4+3645

Baumgartner et al. (2013) identified the brightest XRT source in the field as the counterpart of this BAT source in the Galactic plane. On 2015 June 20, we used modspec to get a spectrum of the optical object nearest to the XRT position, identified in Figure 1, as well as a star $2.''3$ to the north of it. Only the southern star of the pair shows Balmer emission lines and He II $\lambda 4686$ approximately the same strength as $H\beta$, which suggests it is a magnetic CV. The other is an ordinary star.

In 2016 June, we obtained additional spectra. The mean spectrum (Figure 3) again shows Balmer emission lines and He II $\lambda 4686$ approximately the same strength as $H\beta$. The diffuse interstellar bands (DIBs) near $\lambda 5780$ have equivalent widths near 0.6 and 0.8 Å, respectively. The DIBs correlate imperfectly with reddening, but DIBs this strong indicate a reddening $E(B - V)$ greater than 0.5 Å (Lan et al. 2015); at higher reddenings, the DIB strength grows slowly. The reddening map of Green et al. (2015) shows that $E(B - V) = 0.5$ at $d \sim 1.3$ kpc. We tried de-reddening the mean spectrum with various values of $E(B - V)$; for values above 1.0, the continuum appeared bluer than typical unreddened CVs, so this is a rough upper limit, corresponding to $d = 4$ kpc in the Green et al. (2015) map. The map has $E(B - V) = 0.75$ at a true distance modulus $(m - M) = 12$, or $d = 2.5$ kpc;

the apparent $V = 18.7$ would then imply $M_V = +4.3$ [taking $R = A_V/E(B - V) = 3.1$], which is reasonable for a novalike variable.

Although the strength of He II suggests a magnetic CV, 6 hours of time-series photometry obtained 2016 September 2 (Figure 10) did not show any periodic signal. The analysis is made more difficult by the equally bright star only $2''.3$ away.

Our $H\alpha$ radial velocities do not indicate a period unambiguously but do show it to be > 6 hr. The strongest periodicities appear at 0.421 ± 0.002 day and 0.733 ± 0.003 day, with weaker aliases near 0.38 day and 0.86 day. The velocities in Figure 3 are folded on the 0.421-day candidate period, purely for illustration.

3.9. *RX J2015.6+3711*

RX J2015.6+3711 was spectroscopically identified as a likely magnetic CV by Halpern et al. (2001, 2002) because its He II $\lambda 4686$ emission line is comparable in strength to $H\beta$. The ambiguity of the possible identification of this soft source with the hard X-ray source IGR J20159+3713, which corresponds to the BAT source Swift J2015.9+3715/4PBC J2015.5+3711, was reviewed in Paper II (see also Bassani et al. 2014). We did not resolve the identification problem; however, Paper II and Coti Zelati et al. (2016) reported the discovery of a 7215 ± 31 s or 7196 ± 11 s period and its harmonics in the X-ray emission from RX J2015.6+3711.

Paper II interpreted this as the orbital period of a polar, while Coti Zelati et al. (2016) argues that it is the spin period of an IP because the complex pulse shape and its energy dependence is caused by photoelectric absorption, which is typical for IPs. If so, this 2.00 hr period would be the second longest spin period for an IP. In addition, Coti Zelati et al. (2016) identified weak signals in the power spectrum that could correspond to the beat period between the spin and orbit, and used them to infer an orbital period of ≈ 12 hr.

We have spectra of this star from many observing runs starting in 2008. The mean spectrum (Fig. 3) shows Balmer, He I, and He II emission lines on a reddened continuum. The $\lambda 5780$ and $\lambda 6282$ DIBs are both detected. A late-type spectrum appears weakly; we cannot determine a precise spectral type because of the low signal-to-noise ratio, but estimate it to be within a few subclasses of K5. We were able to obtain absorption-line velocities from cross-correlation, which indicated a period near 12.761 hr. While this was discernible in velocities derived from the individual exposures, averaging contiguous exposures into blocks of 20–45 minutes duration gave stronger correlation peaks and smaller velocity uncertainties, so we used these averaged-spectrum velocities in the analysis. An alternate period near 12.570 hr cannot be excluded; it corresponds to one fewer cycle per 34 days. The $H\alpha$ emission velocities show some apparently significant periodicities around a half a day, but none of them agree in detail with the absorption-line period. We adopt the absorption-line period, because (1) the ratio of the absorption-line velocity amplitude to their scatter, K/σ , is much greater than for the emission lines, and (2) the stellar photosphere from which the absorption arises is tied firmly to the secondary star’s orderly motion, while CV emission lines often behave erratically.

The orbital period we find here is consistent with the Coti Zelati et al. (2016) interpretation of the 2.00 hr period as a spin period and is not consistent with our polar suggestion from Paper II. The spectrum also appears consistent with a novalike variable. In particular, $H\alpha$ does not show the phase-dependent, asymmetric line wings characteristic of the accretion columns found in polars.

We applied our Monte Carlo procedure for estimating distance based on the surface brightness and size constraints of the secondary star. The three-dimensional reddening map of Green et al. (2015)

shows an abrupt increase from a very low value to $E(B - V) = 0.4$ at 500 pc, followed by a gradual rise to 0.7 near 3 kpc, and then another abrupt rise to 1.1 before 4 kpc. Happily, the region of gradual rise between 500 pc and 3 kpc coincides with the plausible range of distances; we assumed reddening values in this range and found the distance to be 1400^{+500}_{-400} pc, where the uncertainties are one standard deviation.

3.10. *IGR J21095+4322*

Masetti et al. (2017) identified a star with an emission-line spectrum coincident with this *INTEGRAL*/IBIS source (Bird et al. 2016), which is also the previously unidentified 1RXS J210923.6+431937. It is one of the two stars suggested as candidates by Malizia et al. (2017) based on the position of an X-ray counterpart in the XRT. We obtained spectra of both stars on 2017 May 28 using OSMOS, confirming that only the one identified by Masetti et al. (2017) has emission lines. The other is an ordinary star. As the presence of He II $\lambda 4686$ emission in the spectrum possibly indicates a magnetic CV, we then obtained the two short time series shown in Figure 11. Though rapidly variable, these are inconclusive in that they do not reveal a periodic signal.

In 2017 August, we took four more 12-minute spectra of IGR J21095+4322 with OSMOS. Their sum (Figure 2) shows H α with EW ≈ 23 Å and a rather narrow FWHM of 370 km s $^{-1}$. The signal-to-noise at $\lambda < 5000$ Å was somewhat degraded, but He II $\lambda 4686$ was clearly detected with strength comparable to H β .

3.11. *Swift J2113.5+5422*

This source, corresponding to 1RXS J211336.1+542226, was identified spectrally by Masetti et al. (2010), who tentatively suggested that it might be a magnetic CV on the basis of the detected He II $\lambda 4686$ emission line. We tried for several years to get additional optical data on Swift J2113.5+5422, but found that it was in an extremely low state, much fainter than the $R = 18.8$ listed by Masetti et al. (2010). On 2013 July 4, we measured $V \approx 22.2 \pm 0.2$, too faint for detailed study. It was also faint on 2014 September 29. Finally, in 2016 August and September, the star had returned to its high state, and we obtained the data shown in Figure 12.

Our light curve is similar to the *XMM-Newton* X-ray data of Bernardini et al. (2017), as well as their *V*-band light curve from the *XMM-Newton* OM. Although we cover only 2 cycles of their 4.02 ± 0.10 hr X-ray period, presumed to be the orbital period, the amplitude of our signal is strong, and our period of 4.17 ± 0.10 hr is consistent with theirs. We do not have time-resolved optical spectroscopy of Swift J2113.5+5422 to confirm this as the orbital period.

Other X-ray periods at 1266 s and 1374 s were attributed to the spin and beat period, respectively, but these are not detected in our optical light curve, nor by the OM. From the X-ray spectral behavior, Bernardini et al. (2017) conclude that photoelectric absorption is responsible for both the spin and orbital modulations.

3.12. *Swift J2116.5+5336*

Swift J2116.5+5336 is an unpublished BAT source that corresponds to the previously unidentified 1RXS J211648.0+533349. Using archival XRT images, we identified its optical counterpart using OSMOS on 2017 July 20 to obtain a spectrum of the star closest to the XRT source, as marked in Figure 1. Figure 2 shows the mean spectrum from OSMOS in 2017 August. It shows unusually strong He II emission, with $\lambda 4686$ stronger than H β (their emission EWs are respectively 17 Å and

15 Å); He II $\lambda 5411$ appears with an EW of 8 Å. The lines are single-peaked and broad, with H α having a FWHM of 1300 km s⁻¹.

Time-series photometry over five nights in 2017 September–October (Figure 13) reveals deep eclipses with a period of 0.273 day (6.56 hr) in which ingress and egress of the WD can be clearly identified as the steepest features. The WD ingress and egress times can be timed to a fraction of the 23 s observing cadence and are listed in Table 4. From these, we derive ephemerides (in TDB) of

$$T_{\text{ingress}} = \text{BJD } 2458013.764728(24) + 0.27314731(65) \times E$$

$$T_{\text{egress}} = \text{BJD } 2458013.788482(27) + 0.27314728(74) \times E$$

An expanded view of the eclipses is shown in Figure 14. Emission from the hot spot where the accretion stream impacts the accretion disk contributes to the asymmetry in the eclipse light curve; the hot spot remains visible after the WD dwarf is occulted, and it takes some time to appear again after WD egress.

Despite the strong He II emission, flickering, and eclipse evidence for an accretion disk, we can find no shorter period in the power spectrum that would correspond to an IP spin period.

3.13. *Swift J2138.8+5544*

Swift J2138.8+5544 was discovered serendipitously in XRT images of the field of GRB 050422. Nichelli et al. (2009) found a coherent 989.167(1) s modulation in the X-ray flux from this source, identified the source with an object that showed H and He emission lines, and suggested it was a cataclysmic variable. The optical spectrum varies between our four epochs of observation (2013 September, 2014 October, 2017 August, and 2017 October). In 2013 September, the synthesized *V* magnitude was 19.2, and the emission lines were broader than in subsequent epochs – the FWHM of H α near 1300 km s⁻¹. The source was brighter in 2014 October, and the lines much narrower, near 300 km s⁻¹. At both of these epochs, the radial velocities did not trace a consistent velocity curve. However, in 2017 August and October, the source appeared in an intermediate state (Figure 4), with line widths near 700 km s⁻¹, and the velocities yielded a period of 4.426 ± 0.017 hr, which is likely to be the orbital period.

We obtained time-series photometry of Swift J2138.8+5544 on three consecutive nights in 2017 September. A GG420 filter was used with Templeton. The results in Figure 15 show regular pulsations at a period of 989.43 ± 0.30 s in the coherent power spectrum, consistent with the X-ray value of Nichelli et al. (2009). In addition, there is a strong peak at 4.36 ± 0.02 hr, very close to the spectroscopic value of 4.426 ± 0.017 hr. Therefore, we regard this as confirmation of the spectroscopic period.

3.14. *Swift J2237.2+6324*

This CV with strong He II $\lambda 4686$ emission was identified by Lutovinov et al. (2012). Our data in Figure 16 do not reveal an obvious period, although the long light curve of 2016 September 3 has a large ~ 8 hr modulation that may represent the orbital period. We do not have time-resolved spectroscopy of Swift J2237.2+6324 to test this conjecture.

3.15. *1SWXRT J230642.7+550817*

This source from the latest *INTEGRAL*/IBIS catalog (Bird et al. 2016) is identified with 1RXS J230645.0+550816 and was classified as a CV in Landi et al. (2017), with details of the optical spectrum stated to appear in a later paper. We obtained time-series photometry of the identified star on five nights in 2017 June. A *V* filter was used with Templeton (20 s exposures) or a GG420 filter with Andor (30 s exposures). Figure 17 shows regular pulsations from 1SWXRT J230642.7+550817, demonstrating that it is a new IP. It was possible to phase connect all of the data, yielding a period of 464.452 ± 0.004 s.

We have time-series spectroscopy from several runs in the 2017 season, but the coverage was not sufficient to determine a firm period. The most likely period is near 0.136 day, but other daily cycle-count aliases and some much longer periods remain possible. Figure 4 shows the spectrum, periodogram, and a purely illustrative folding of the velocities on the strongest candidate period.

4. CONCLUSIONS

We identified 4 new CV counterparts of the *Swift* BAT survey or *INTEGRAL*/IBIS sources, and we obtained time-resolved spectroscopy or photometry on an additional 11 that were previously known. Three are new IPs based on spin periods detected in their photometry: Swift J0535.2+2830 (1523 s), 2PBC J1911.4+1412 (747 s), and 1SWXRT J230642.7+550817 (464 s). Of these, 2PBC J1911.4+1412 had previously been suggested to be a low-mass X-ray binary. We also confirmed and refined spin periods in three systems. We discovered two eclipsing systems: Swift J2116.5+5336 and the new polar 2PBC J0658.0–1746.

We found exact or approximate spectroscopic orbital periods for six additional targets. The 4.63-day orbit for Swift J0623.9–0939, which is revealed by the radial velocities of the photospheric absorption lines of the K-type secondary star, is the second longest known CV period. We also discover a 12.76-hr orbital period for RX J2015.6+3711 in photospheric absorption lines, which confirms that the previously detected 2.00 hr X-ray period from this star is the spin period of an IP, as inferred by Coti Zelati et al. (2016).

With the caveat that the the small set of CVs studied here is not a well-defined sample, these results are consistent with previous investigations that show hard X-ray selection favoring magnetic over non-magnetic CVs, and IPs outnumbering polars. This is both because IPs have higher accretion rates, and because in polars, some fraction of the accretion energy appears as soft X-rays from the WD surface.

MDM Observatory is operated by Dartmouth College, Columbia University, the Ohio State University, Ohio University, and the University of Michigan. J.R.T. gratefully acknowledges support from NSF grant AST-1008217. This work has made use of data from the European Space Agency (ESA) mission *Gaia* (<https://www.cosmos.esa.int/gaia>), processed by the *Gaia* Data Processing and Analysis Consortium (DPAC, <https://www.cosmos.esa.int/web/gaia/dpac/consortium>). Funding for the DPAC has been provided by national institutions, in particular the institutions participating in the *Gaia* Multilateral Agreement.

REFERENCES

- | | |
|---|--|
| <p>Alam, S., Albareti, F. D., Allende Prieto, C., et al. 2015, <i>ApJS</i>, 219, 12</p> | <p>Altmann, M., Roeser, S., Demleitner, M., Bastian, U., & Schilbach, E. 2017, <i>A&A</i>, 600, L4</p> |
|---|--|

- Bassani, L., Landi, R., Malizia, A., et al. 2014, *A&A*, 561, A108
- Baumgartner, W. H., Tueller, J., Markwardt, C. B., et al. 2013, *ApJS*, 207, 19
- Benedict, G. F., Henry, T. J., Franz, O. G., et al. 2016, *AJ*, 152, 141
- Bernardini, F., de Martino, D., Mukai, K., et al. 2017, *MNRAS*, 470, 4815
- Bessell, M. S. 1990, *PASP*, 102, 1181
- Bird, A. J., Bazzano, A., Malizia, A., et al. 2016, *ApJS*, 223, 15
- Coppejans, R., Gulbis, A. A. S., Kotze, M. M., et al. 2013, *PASP*, 125, 976
- Coti Zelati, F., Rea, N., Campana, S., et al. 2016, *MNRAS*, 456, 1913
- Cusumano, G., La Parola, V., Segreto, A., et al. 2010, *A&A*, 524, A64
- Eastman, J., Siverd, R., & Gaudi, S. B. 2010, *PASP*, 122, 935
- Gaia Collaboration, Prusti, T., de Bruijne, J. H. J., et al. 2016a, *A&A*, 595, A1
- Gaia Collaboration, Brown, A. G. A., Vallenari, A., et al. 2016b, *A&A*, 595, A2
- Green, G. M., Schlafly, E. F., Finkbeiner, D. P., et al. 2015, *ApJ*, 810, 25
- Halpern, J. P., Bogdanov, S., & Thorstensen, J. R. 2017, *ApJ*, 838, 124
- Halpern, J. P., Eracleous, M., Mukherjee, R., & Gotthelf, E. V. 2001, *ApJ*, 551, 1016
- Halpern, J. P., Eracleous, M., Mukherjee, R., & Gotthelf, E. V. 2002, *ApJ*, 572, 693
- Halpern, J. P., & Thorstensen, J. R. 2015, *AJ*, 150, 170, (Paper II)
- Henden, A. A., Levine, S. E., Terrell, D., Smith, T. C., & Welch, D. 2012, *JAVSO*, 40, 430
- Horne, K. 1986, *PASP*, 98, 609
- Kalomeni, B., Nelson, L., Rappaport, S., et al. 2016, *ApJ*, 833, 83
- Knigge, C. 2011, in *ASP Conf. Ser.* 447, *Evolution of Compact Binaries*, ed. L. Schmidtbreick, M. R. Schreiber, & C. Tappert (San Francisco, CA: ASP), 3
- Lan, T.-W., Ménard, B., & Zhu, G. 2015, *MNRAS*, 452, 3629
- Landi, R., Bassani, L., Bazzano, A., et al. 2017, *MNRAS*, 470, 1107
- Lutovinov, A. A., Burenin, R. A., Revnivtsev, M. G., et al. 2012, *AstL*, 38, 281
- Malizia, A., Landi, R., Bassani, L., et al. 2017, *ATel* 10364
- Martini, P., Stoll, R., Derwent, M. A., et al. 2011, *PASP*, 123, 187
- Masetti, N., Malizia, A., Landi, R., et al. 2017, *ATel* 10447
- Masetti, N., Parisi, P., Palazzi, E., et al. 2010, *A&A*, 519, A96
- Monet, D. G., Levine, S. E., Canzian, B., et al. 2003, *AJ*, 125, 984
- Nichelli, E., Israel, G. L., Moretti, A., et al. 2009, *ATel*, 2354
- Parisi, P., Masetti, N., Rojas, A. F., et al. 2014, *A&A*, 561, A67
- Ritter H., & Kolb U. 2003, *A&A*, 404, 301 (update RKcat7.24, 2016)
- Rojas, A. F., Masetti, N., Minniti, D., et al. 2017, *A&A*, 602, A124
- Scargle, J. 1982, *ApJ*, 263, 835
- Schneider, D., & Young, P. 1980, *ApJ*, 238, 946
- Shafter, A. W. 1983, *ApJ*, 267, 222
- Sirk, M. M., & Howell, S. B. 1998, *ApJ*, 506, 824
- Thorstensen, J. R., & Freed, I. W. 1985, *AJ*, 90, 2082
- Thorstensen, J. R., & Halpern, J. 2013, *AJ*, 146, 107, (Paper I)
- Thorstensen, J. R., Patterson, J., Thomas, G., & Shambrook, A. 1996, *PASP*, 108, 73
- Tovmassian, G., González-Buitrago, D., Thorstensen, J., et al. 2017, *A&A*, 608, A36
- Warren, J. K., Sirk, M. M., & Vallergera, J. V. 1995, *ApJ*, 445, 909
- Zacharias, N., Finch, C. T., Girard, T. M., et al. 2013, *AJ*, 145, 44

Table 1. Basic Data on Stars Observed

Name	R.A. ^a (h m s)	Decl. ^a (° ' ")	V	Ref ^b	g^c	Data ^d	Class ^e	P_{orb} (day)	P_{spin} (s)	Ref ^f
Swift J0535.2+2830	05 34 57.918	+28 28 37.22	19.1	B	19.8	I, T	DQ		1523.07(9)	1
Swift J0623.9−0939	06 24 06.189	−09 38 52.13	14.1	A	14.7	S		4.637(8)		1
2PBC J0658.0−1746	06 58 05.873	−17 44 24.40	16.2	B	16.7	T	AM	0.0991370(3)	$= P_{\text{orb}}$	1
Swift J0717.8−2156	07 17 48.260	−21 53 01.50	18.9	S	17.9	S		0.2298(10)		1
2PBC J0801.2−4625	08 01 17.023	−46 23 27.45	14.9	B		T	DQ		1307.55(10)	1
									1310.9(1.5)	2
									1306.3(0.9)	3
Swift J0927.7−6945	09 27 53.073	−69 44 41.91	16.1	B		T	DQ	0.2021(8)	1033.05(15)	1
								0.219(19)	1033.54(51)	2
									1030.6(9)	3
2PBC J1911.4+1412	19 11 24.872	+14 11 44.86	18.3	B	19.3	T	DQ		746.885(8)	1
Swift J2006.4+3645	20 06 22.395	+36 41 43.57	18.4	S	18.7	I, S, T		0.421 ::		1
RX J2015.6+3711	20 15 36.959	+37 11 22.94	18.1	D	18.6	S	DQ	0.531713(3)	7196(11)	1, 4, 5
IGR J21095+4322	21 09 23.863	+43 19 37.10	18.1	D	18.3	I, T				
Swift J2113.5+5422	21 13 35.397	+54 22 32.95	18.3	B	19.1	T	DQ	0.174(4)	1265.6(4.5)	1, 2
Swift J2116.5+5336	21 16 46.612	+53 33 53.99	16.7	D	18.0	I, T		0.2731473(7)		1
Swift J2138.8+5544	21 38 49.910	+55 44 05.67	18.5	D	18.8	S, T	DQ	0.1843(7)	989.43(30)	1
									989.167(1)	6
Swift J2237.2+6324	22 36 37.401	+63 29 33.60	19.7	D	20.1	T		$\sim 0.33 ::$		1
1SWXRT J230642.7+550817	23 06 42.687	+55 08 20.11	16.9	D	17.1	S, T	DQ	0.136 ::	464.452(4)	1

^aCoordinates are from the *Gaia* first data release (Gaia Collaboration et al. 2016a,b). They are referred to ICRS (essentially equinox J2000), but are for epoch 2015.0 (i.e., for proper motion correction).

^bSource of approximate V magnitude: A—APASS (Henden et al. 2012), as listed in the UCAC4 (Zacharias et al. 2013); B—interpolated from Schmidt-plate magnitudes in USNO B1.0 (Monet et al. 2003); D—our direct image; S—our spectrophotometry.

^cAverage g magnitude from Pan-STARRS.

^dTypes of data presented here: I—optical spectroscopic identification; S—time-resolved spectroscopy; T—time-series photometry.

^eClassifications are: AM—AM Her star or polar; DQ—DQ Her star or IP (evidence for pulsations).

^fReferences for periods: (1) this paper, optical; (2) Bernardini et al. 2017, X-ray; (3) Bernardini et al. 2017, optical; (4) Paper II, X-ray; (5) Coti Zelati et al. 2016, X-ray; (6) Nichelli et al. 2009, X-ray.

Table 2. Radial Velocities

Star	Time	v_{eml}	σ	v_{abs}	σ
	(days)	(km s ⁻¹)	(km s ⁻¹)	(km s ⁻¹)	(km s ⁻¹)
Swift J0623	57402.7147	52	1	-48	11
Swift J0623	57402.7220	52	1	-51	10
Swift J0623	57402.7294	55	1	-49	10
Swift J0623	57405.6506	-6	3	91	13

NOTE—Radial velocities of H α and (when measured) the late-type absorption spectrum. The time given is the barycentric Julian date of mid-integration, minus 2,440,000.0, on the UTC system. (A portion is shown here for guidance regarding its form and content.) (This table is available in its entirety in machine-readable form.)

Table 3. Fits to Radial Velocities

Data Set		T_0^a	P_{spec} (day)	K (km s ⁻¹)	γ (km s ⁻¹)	N	σ^b (km s ⁻¹)
Swift J0623.9–0939	abs	57431.66(2)	4.637(8)	76(3)	26(2)	42	8
	emn	57429.82(13)	...	28(4)	28(3)	43	10
Swift J0717.8–2156		57434.705(4)	0.2298(10)	64(5)	110(4)	23	14
RX J2015.6+3711	abs	55073.854(6)	0.531717(3)	191(14)	–31(11)	26	36
	emn	55128.427(15)	...	98(19)	–46(13)	28	45
Swift J2138.8+5544		58036.605(4)	0.1843(7)	61(7)	11(5)	54	18

NOTE—Parameters of least-squares fits to the radial velocities, of the form $v(t) = \gamma + K \sin [2\pi(t - T_0)/P_{\text{spec}}]$.

^aHeliocentric Julian date minus 2,400,000.0, on the UTC system. The epoch is chosen to be near the center of the time interval covered by the data and within one cycle of an actual observation.

^bRoot-mean-square residual of the fit.

Table 4. Eclipse Timings

Cycle	Ingress	Egress
2PBC J0658.0–1746		
–51	...	2458097.81053
–50	2458097.90273	2458097.90976
–1	2458102.76002	2458102.76740
0	2458102.85918	2458102.86657
1	2458102.95834	2458102.96575
59	...	2458108.71567
60	2458108.80739	2458108.81476
61	2458108.90654	2458108.91393
714	2458173.64085	2458173.64826
715	2458173.73918	...
Swift J2116.5+5336		
–18	2458008.84811	2458008.87193
–11	2458010.76018	2458010.78378
–7	2458011.85264	2458011.87643
–4	2458012.67208	2458012.69588
0	2458013.76473	2458013.78849
88	2458037.80170	2458037.82545

NOTE—Times are Julian date in barycentric dynamical time (TDB).

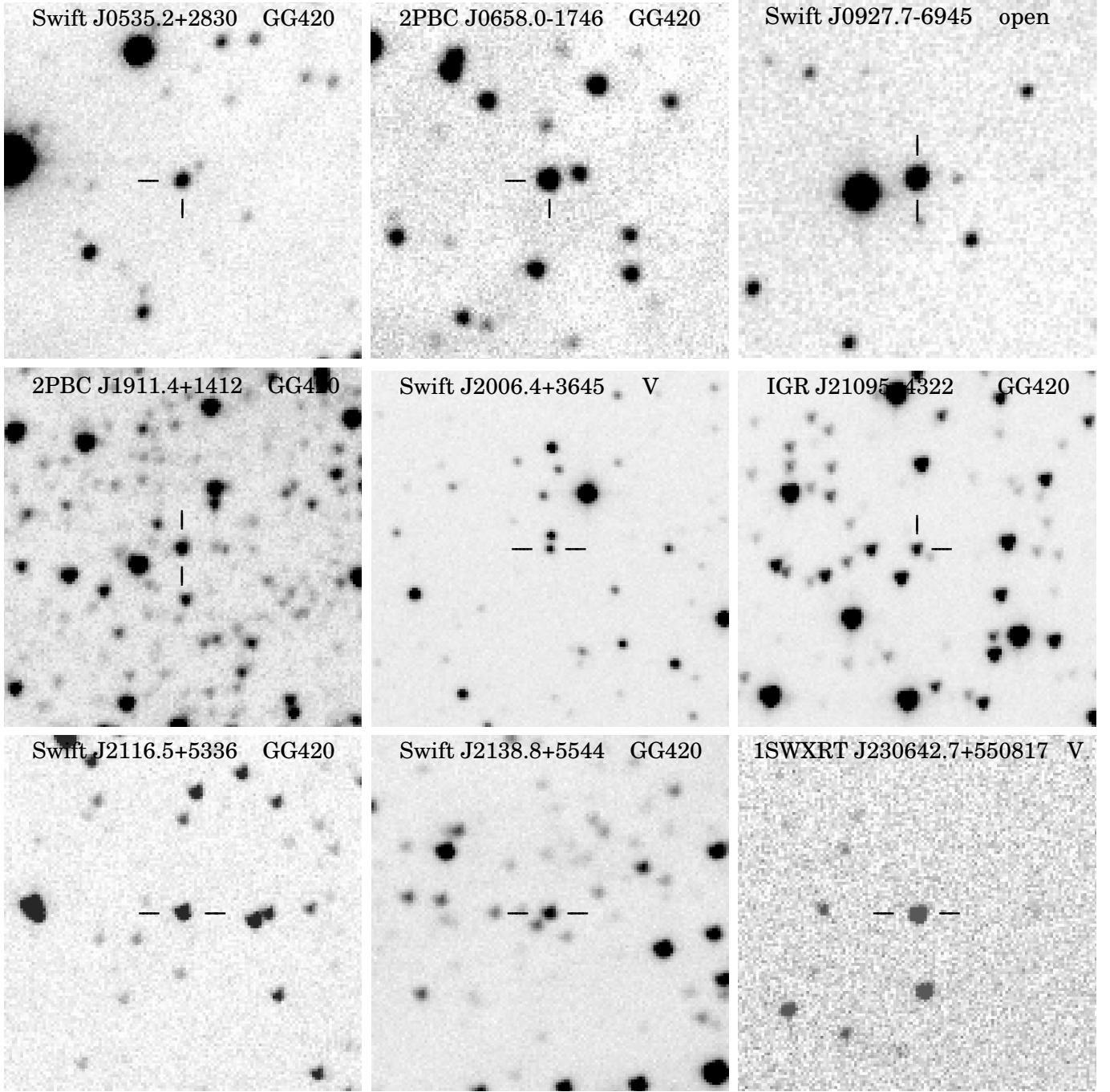


Figure 1. Finding charts for selected objects. All were taken with the MDM 1.3 m, except for Swift J0927.7–6945, which is from the SAAO 1 m. Each field is $1'.1 \times 1'.1$. North is up and east is to the left.

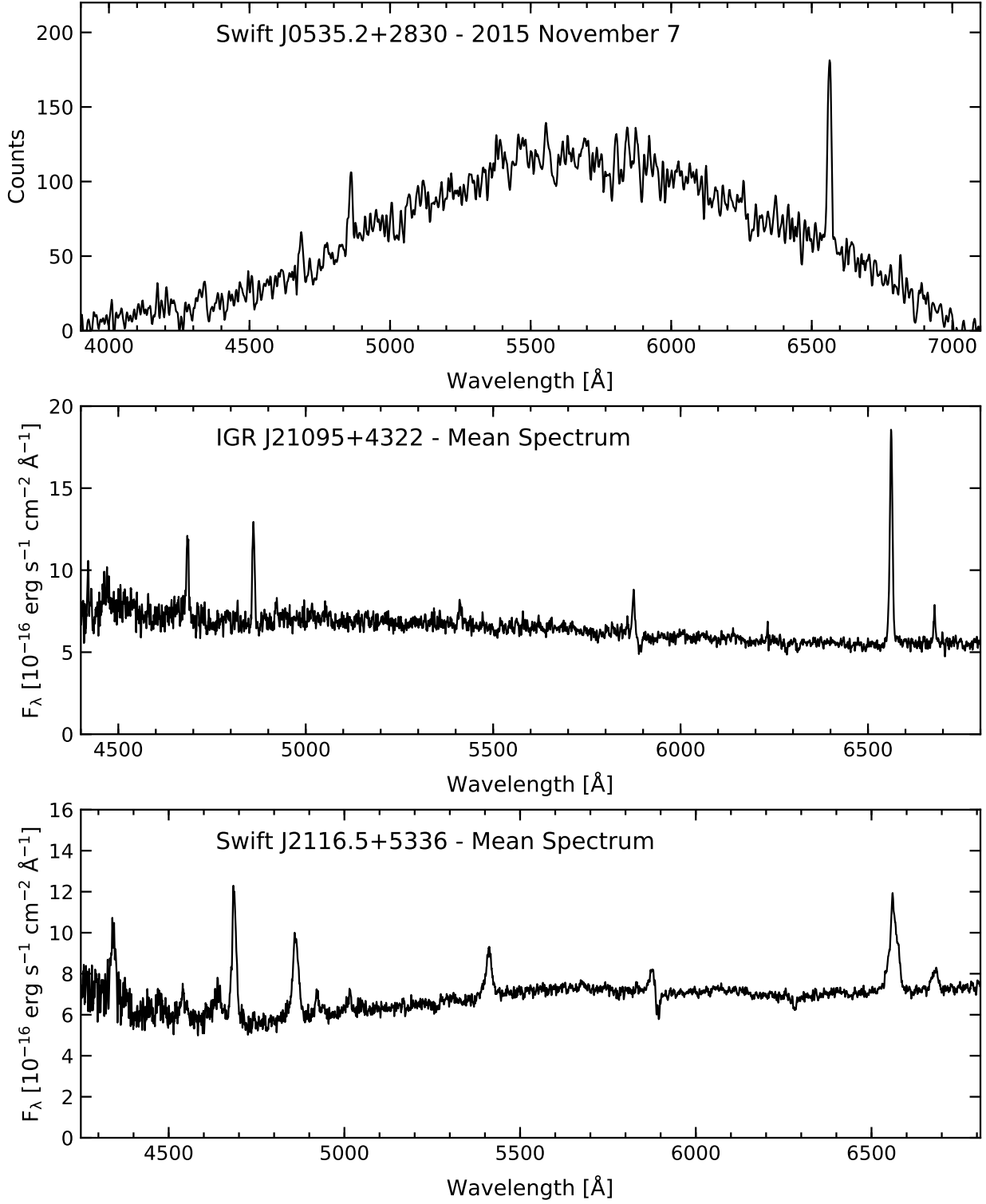


Figure 2. Spectra of Swift J0535.2+2830, IGR J21095+4322, and Swift J2116.5+5336 taken with the MDM 2.4 m. The single spectrum of Swift J0535.2+2830 was taken in 2015 November with the modspec and was not flux-calibrated; the other two spectra are averages from 2017 August using OSMOS. All were smoothed with a three-point average.

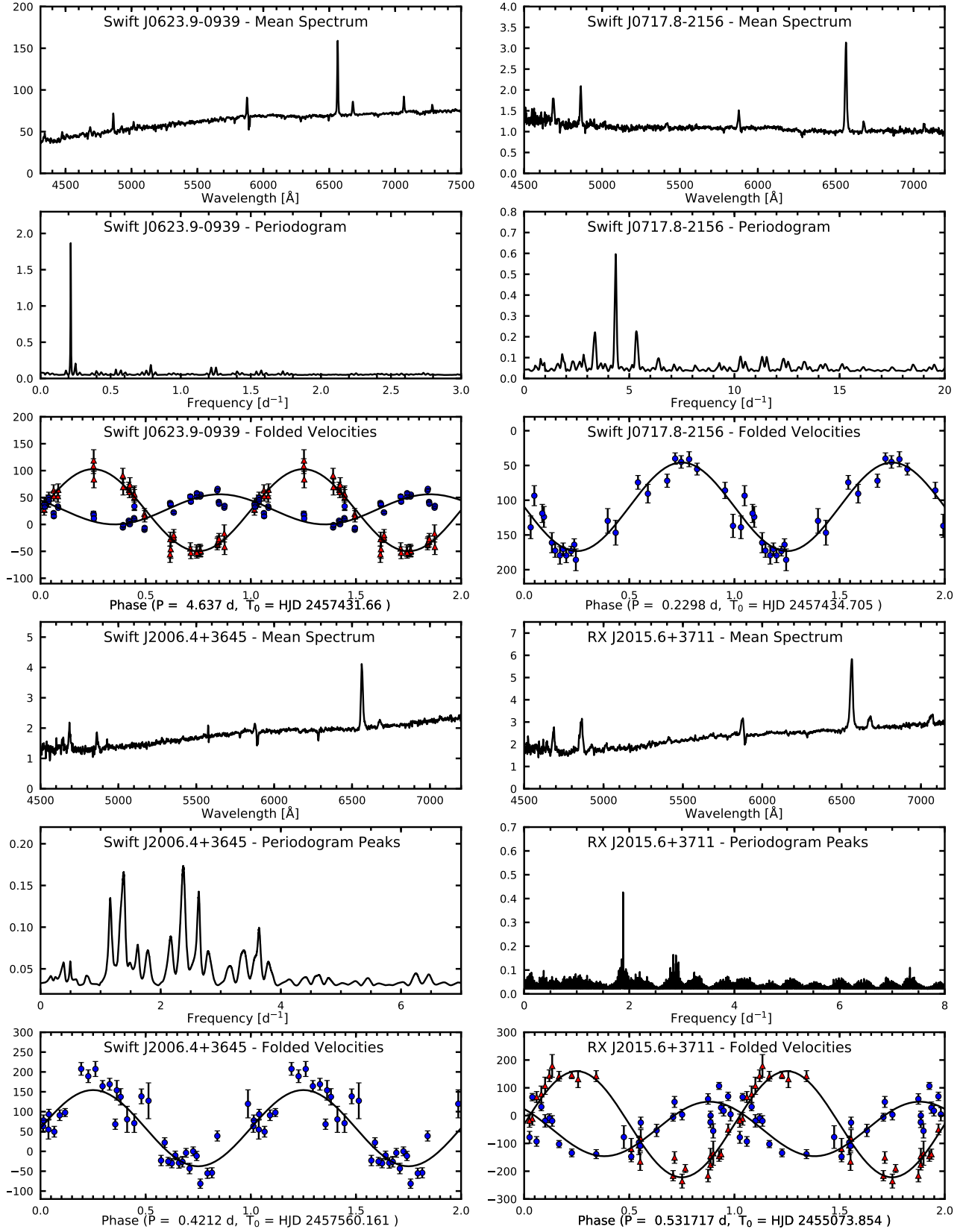
Figure 3. *Caption on next page.*

Figure 3. Average spectra, periodograms, and folded velocity curves for Swift J0623.9–0939, Swift J0717.8–2156, Swift J2006.4+3645, and RX J2015.6+3711. The vertical scales, unlabeled to save space, are (1) for the spectra, f_λ in units of 10^{-16} erg s $^{-1}$ cm $^{-2}$ Å $^{-1}$; (2) for the periodograms, $1/\chi^2$ (dimensionless); and (3) for the radial velocity curves, barycentric radial velocity in km s $^{-1}$. When two traces are shown in the spectral plot, the lower trace shows the average spectrum minus a late-type spectrum scaled to match the spectrum of the secondary star. In cases where velocities are from more than one observing run, the periodogram is labeled with the word “peaks,” because the curve shown is formed by joining local maxima in the full periodogram with straight lines. This suppresses some of the fine-scale ringing due to the unknown number of cycle counts between runs. The folded velocity curves all show the same data plotted over two cycles for continuity, and the best-fit sinusoid (see Table 3) is also plotted. The velocities shown are normally H α emission velocities. Secondary-star cross-correlation velocities, when available, are shown in red, together with the best-fit sinusoid (in which case the period and epoch used in the fold are from the fit to the absorption velocities). The error bars for the emission lines are computed by propagating the estimated noise in the spectrum through the measurement and hence do not include jitter due to line profile variations.

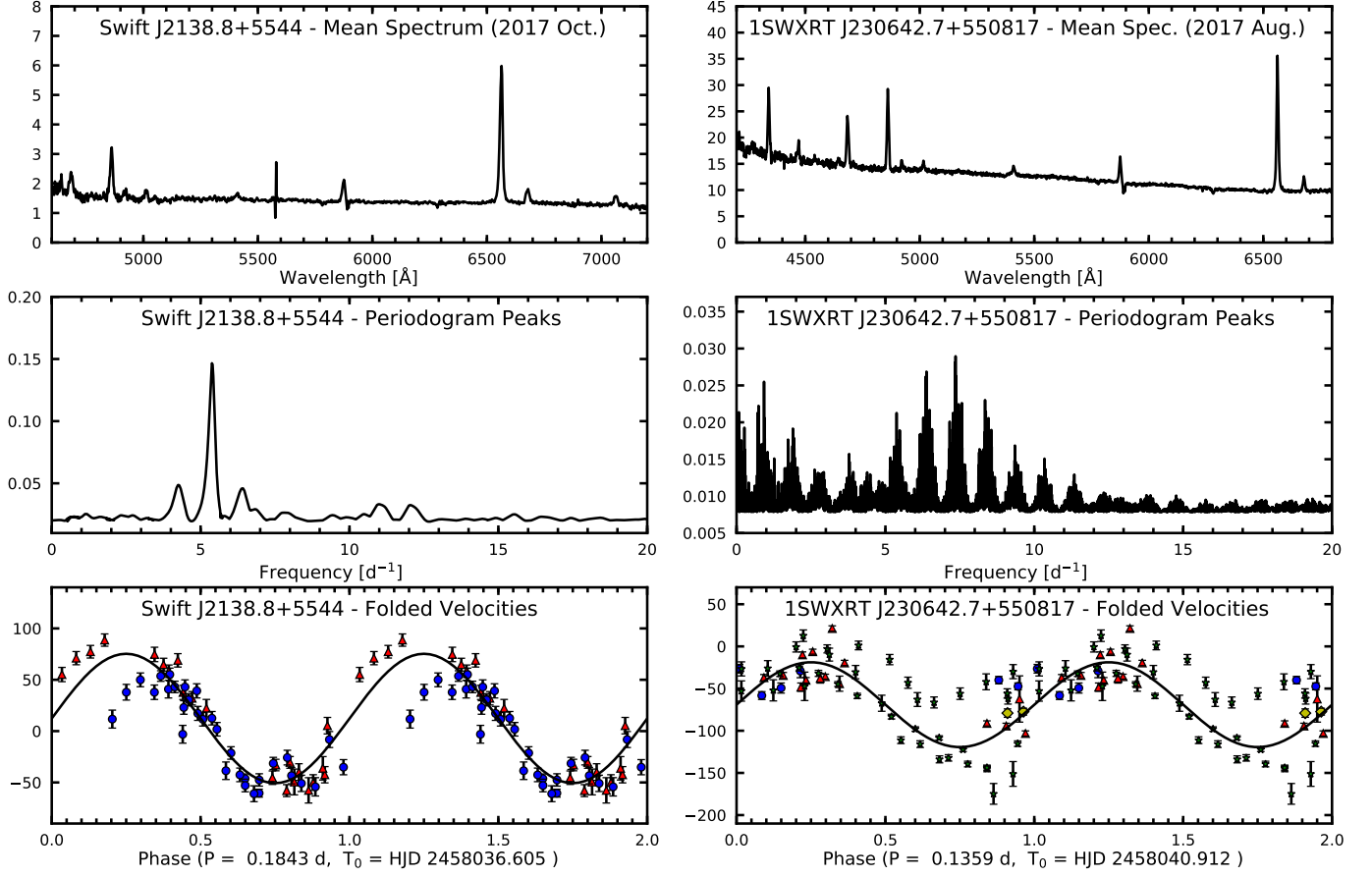


Figure 4. Similar to Figure 3, but for Swift J2138.8+5544 and 1SWXRT J230642.7+550817. For the folded velocities, the symbols represent different observing runs as follows. Yellow diamonds: 2017 June; red triangles: 2017 August; blue circles: 2017 October; green stars: 2017 November. The orbital period of 1SWXRT J230642.7+550817 is not determined unambiguously; the fold shown in the lower-right panel uses the period corresponding to the (barely) highest peak in the periodogram.

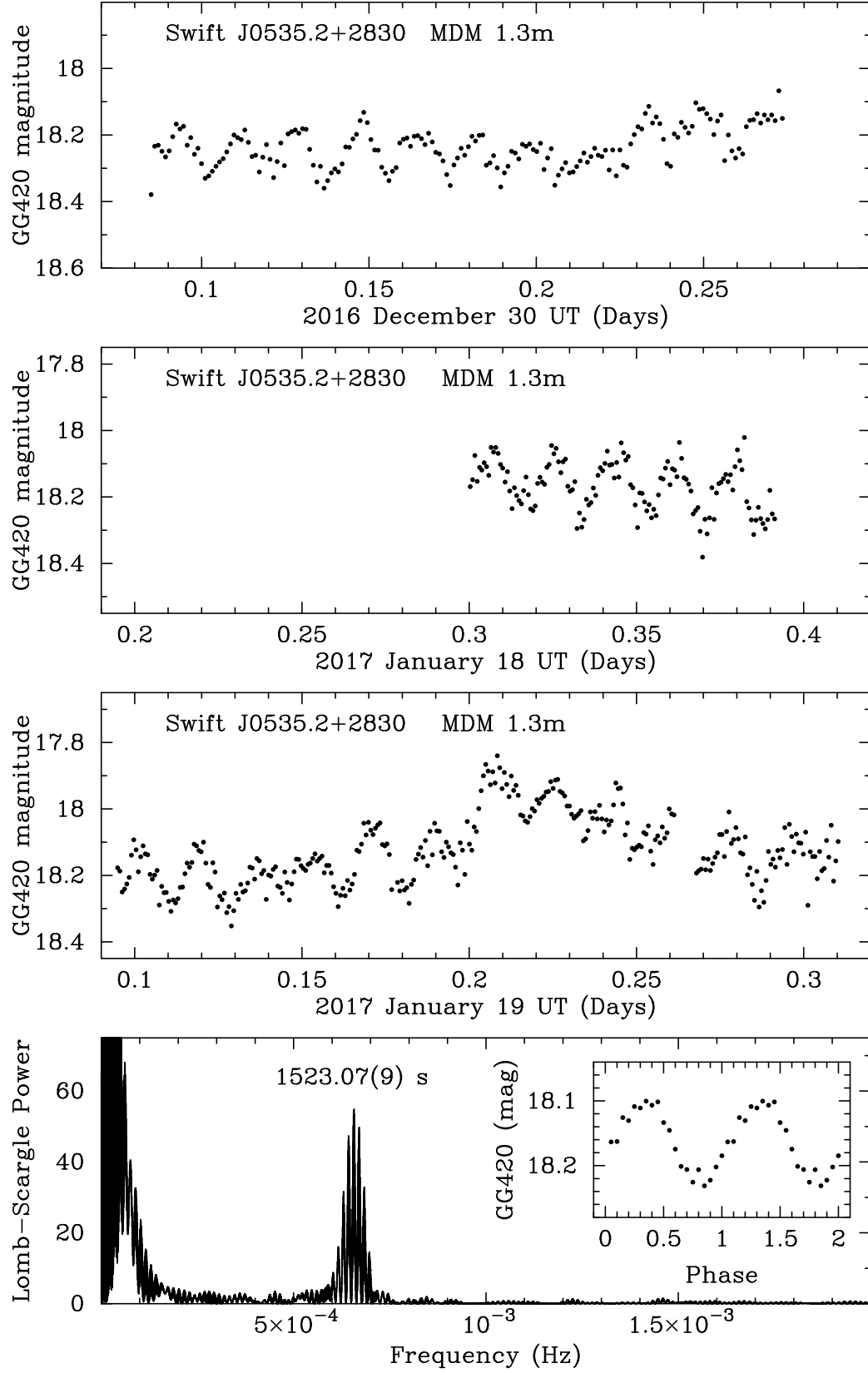


Figure 5. Time-series photometry of Swift J0535.2+2830. Individual exposures are 90 s on December 30 and 60 s on January 18, 19. The inset shows the light curve folded at $P = 1523.07$ s.

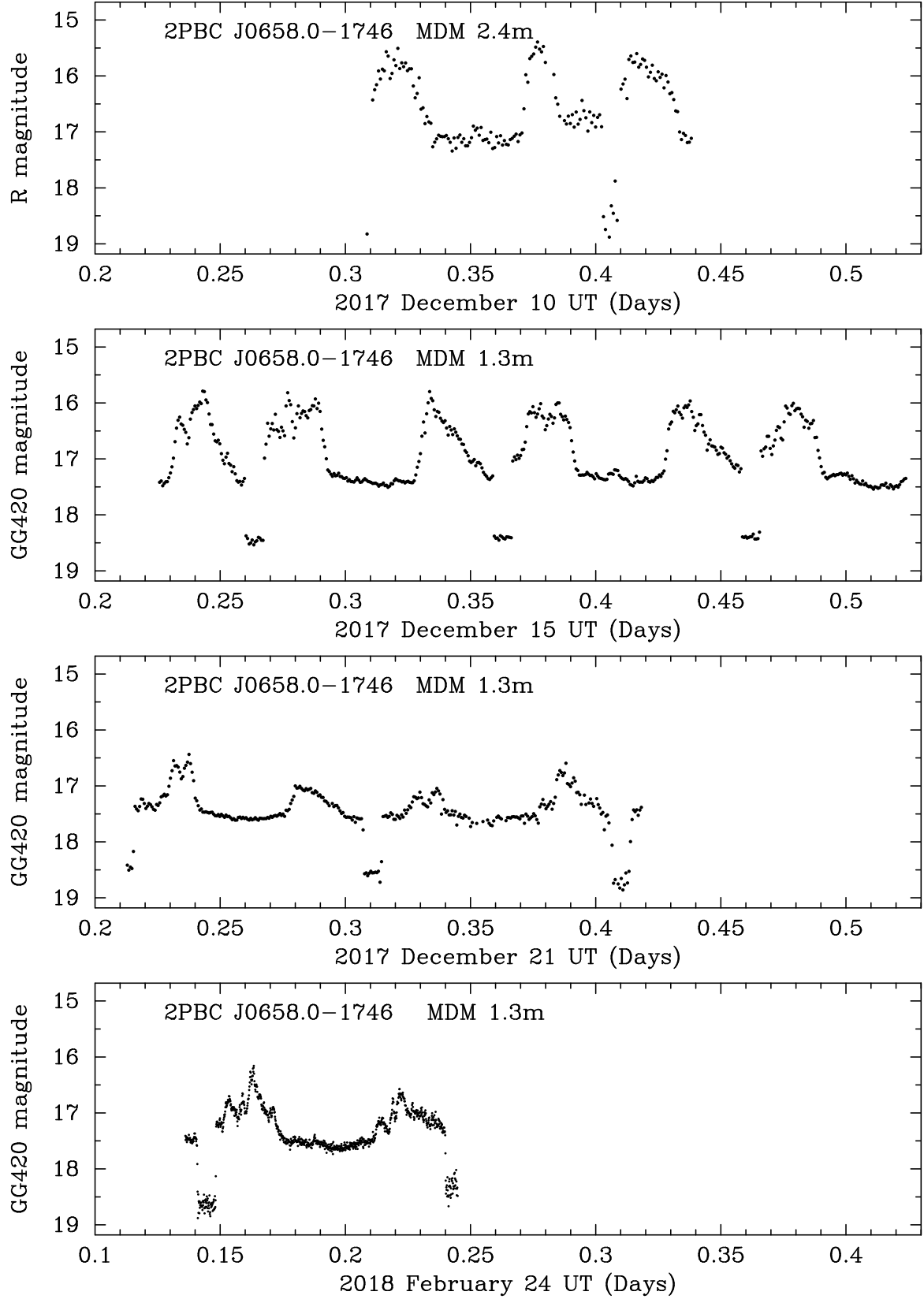


Figure 6. Time-series photometry of 2PBC J0658.0-1746. Individual exposures are 40 s on December 10, 50 s on December 15, 21, and 10 s on February 24. Note in particular the eclipse egress at the beginning of the December 10 observation. Data quality in eclipse was compromised by detector noise on December 10 and by wind shake on December 21, but all eclipses are precisely timed. Eclipse ingress and egress times are listed in Table 4.

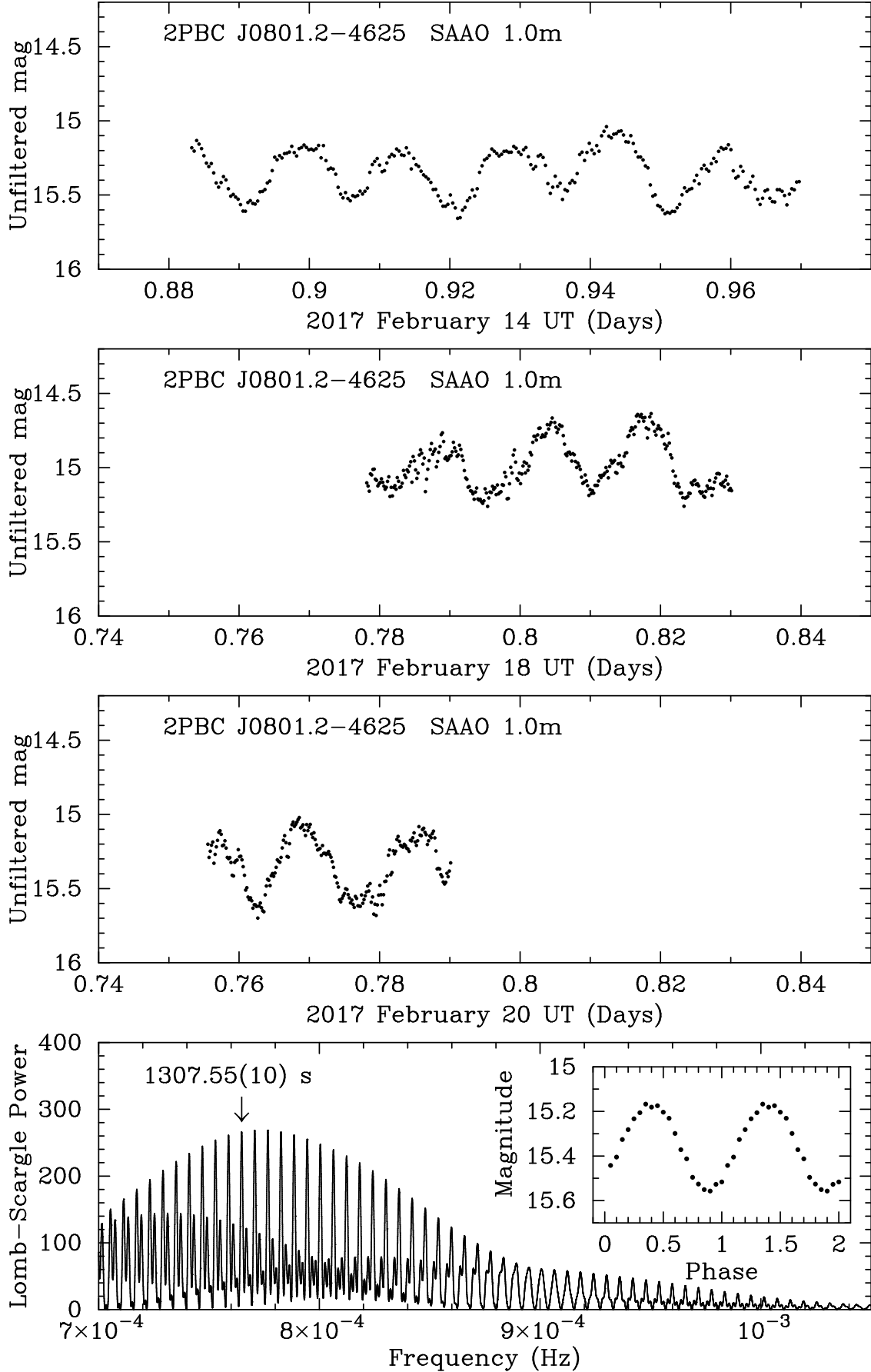


Figure 7. Time-series photometry of 2PBC J0801.2-4625 in unfiltered light. Individual exposures are 30 s. The inset shows the light curve folded at $P = 1307.55$ s, the peak consistent with the X-ray measured period.

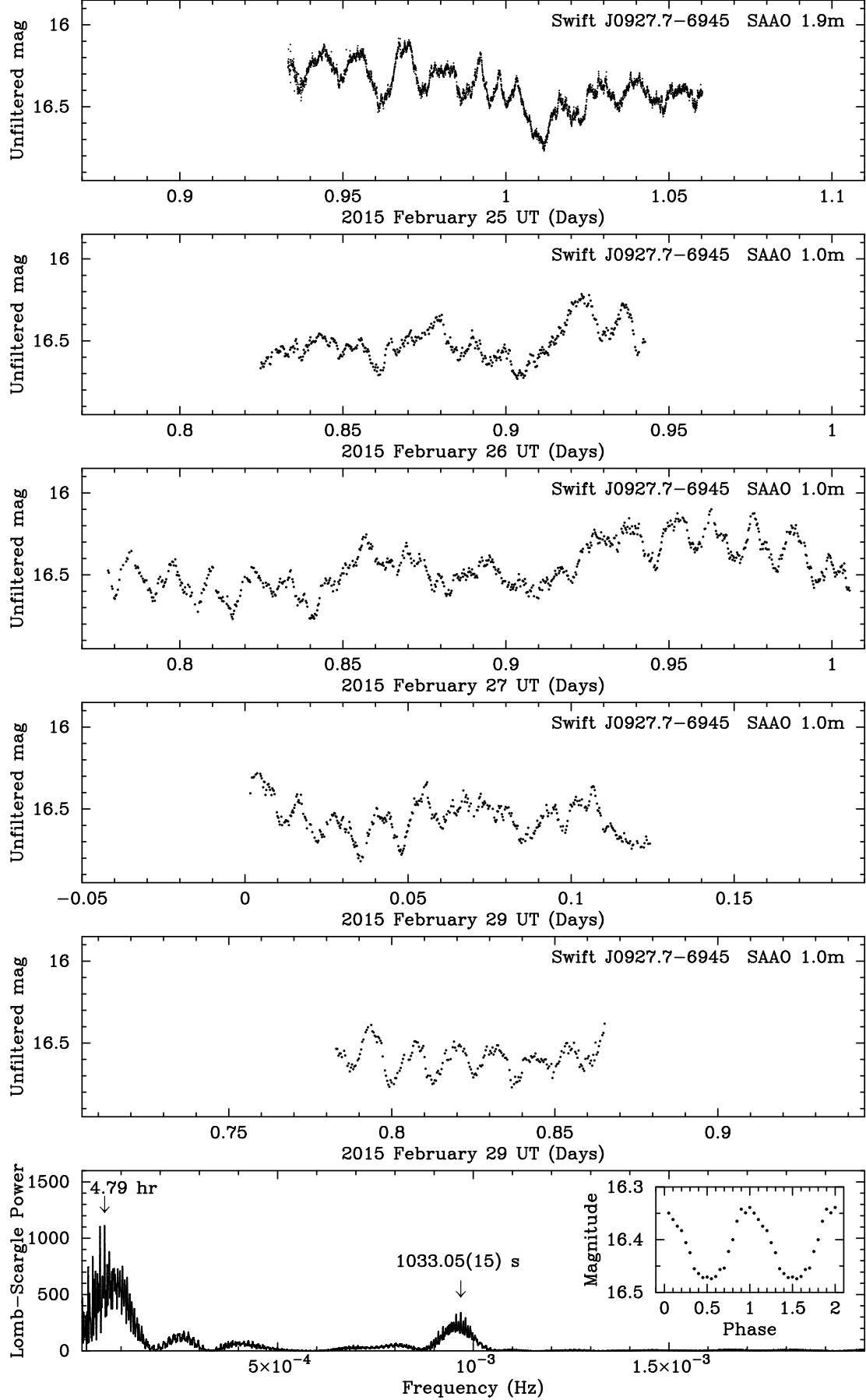


Figure 8. Time-series photometry of Swift J0927.7-6945. Individual exposures range from 2.5 s (top panel) to 30 s (bottom panel) with 20 s for the other three. The inset shows the light curve folded at $P = 1033.05$ s.

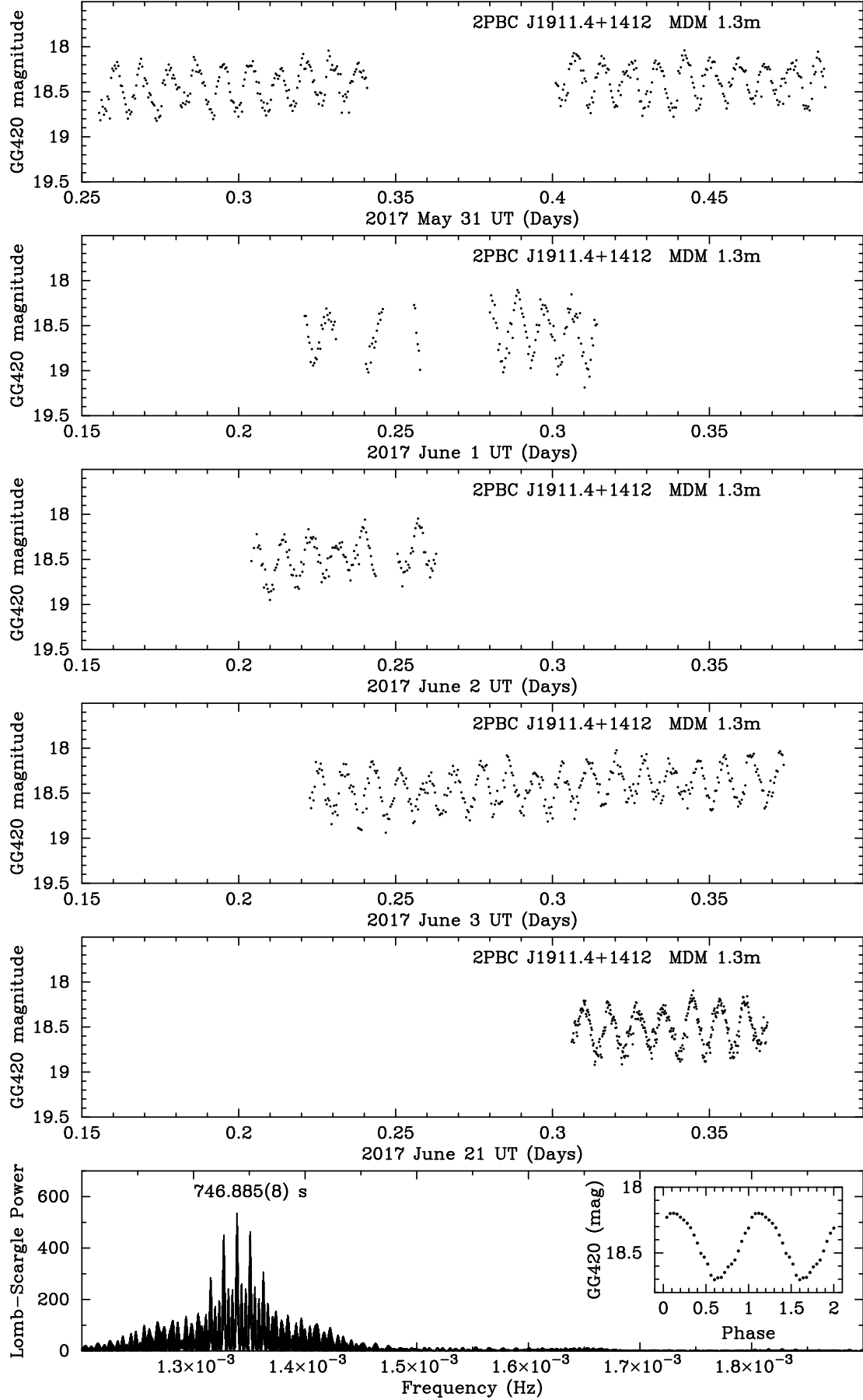


Figure 9. Time-series photometry of 2PBC J1911.4+1412. Individual exposures are 30 s, except for June 21 when they are 15 s. The inset shows the light curve folded at $P = 746.885$ s.

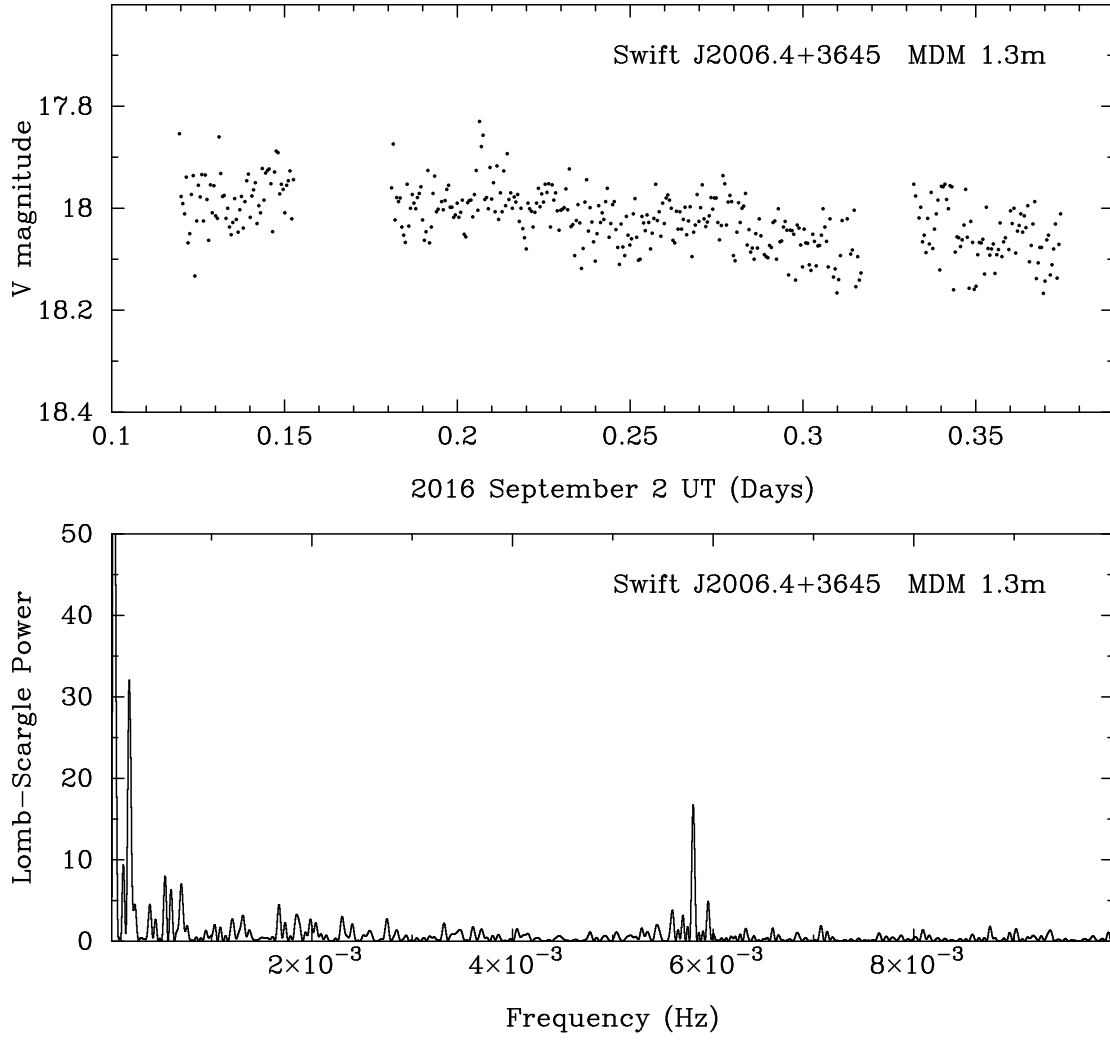


Figure 10. Time-series photometry of Swift J2006.4+3645. Individual exposures are 40 s. The peak in the power spectrum at 5.8×10^{-3} Hz is an artifact, being at half the Nyquist frequency ($4 \times$ the sampling period).

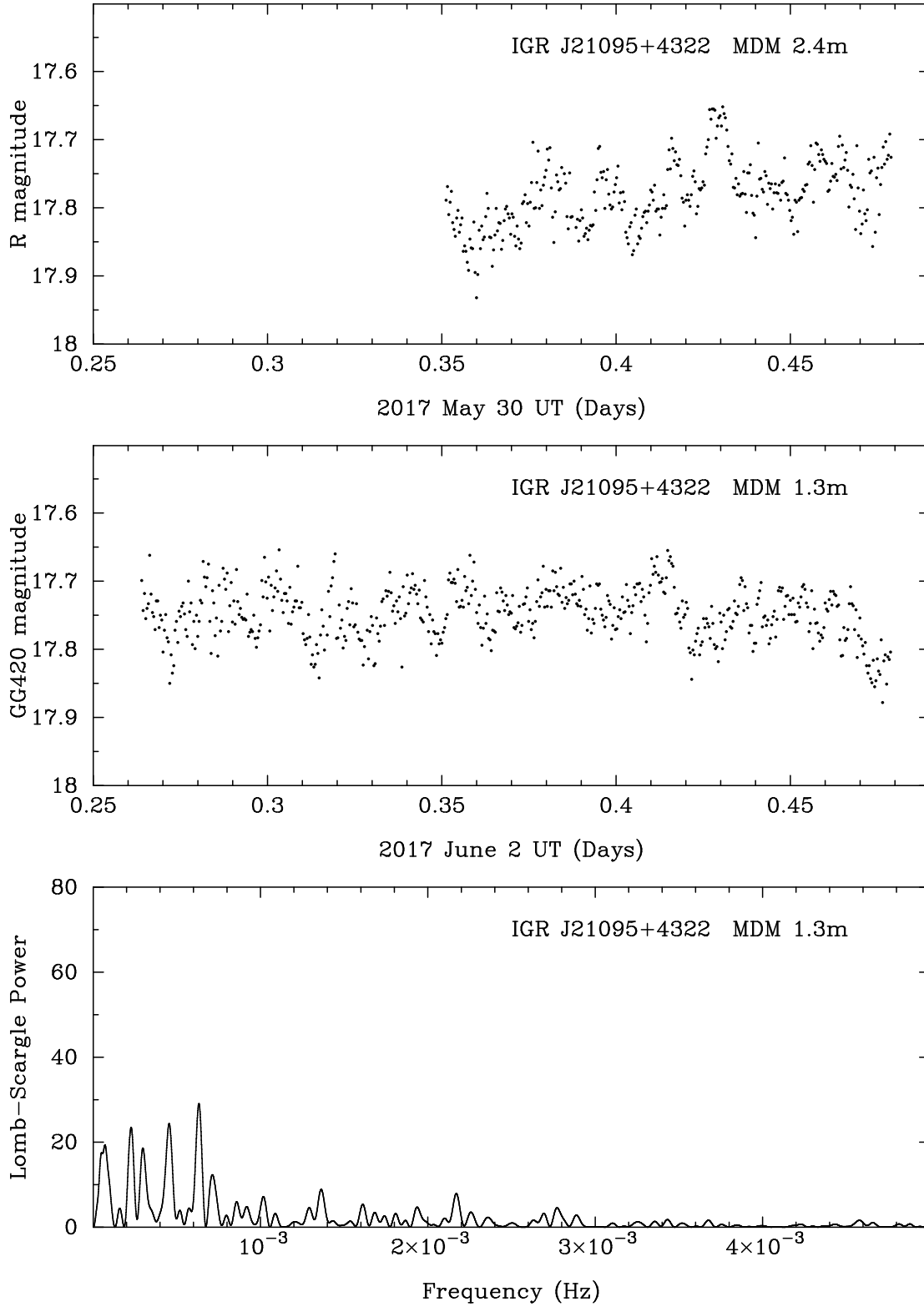


Figure 11. Time-series photometry of IGR J21095+4322. Individual exposures are 30 s. The power spectrum is of the June 2 data only.

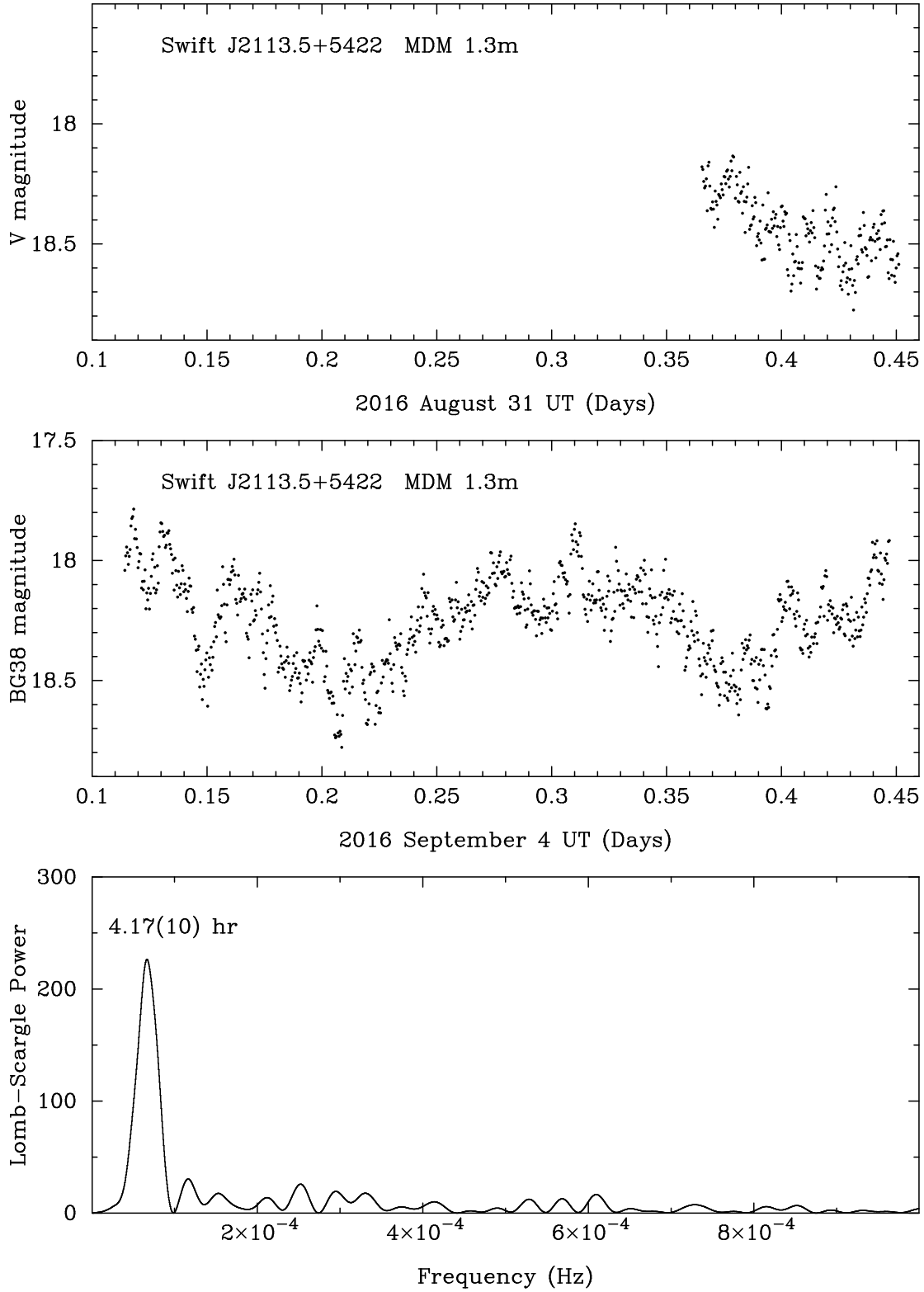


Figure 12. Time-series photometry of Swift J2113.5+5422. Individual exposures are 30 s. The power spectrum is of the September 4 data only.

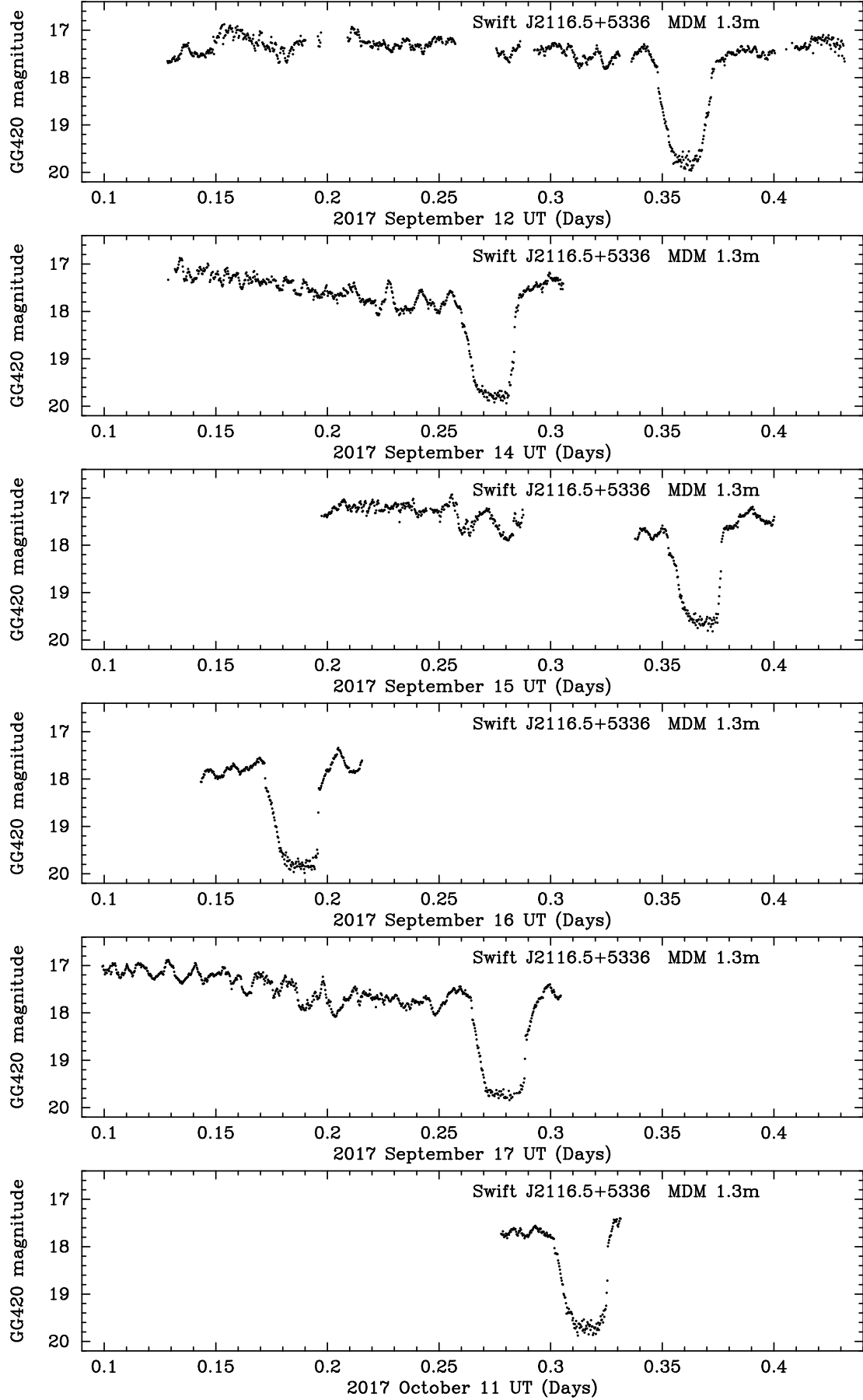


Figure 13. Time-series photometry of Swift J2116.5+5336. Individual exposures are 20 s. Eclipse timings are listed in Table 4. See also Figure 14.

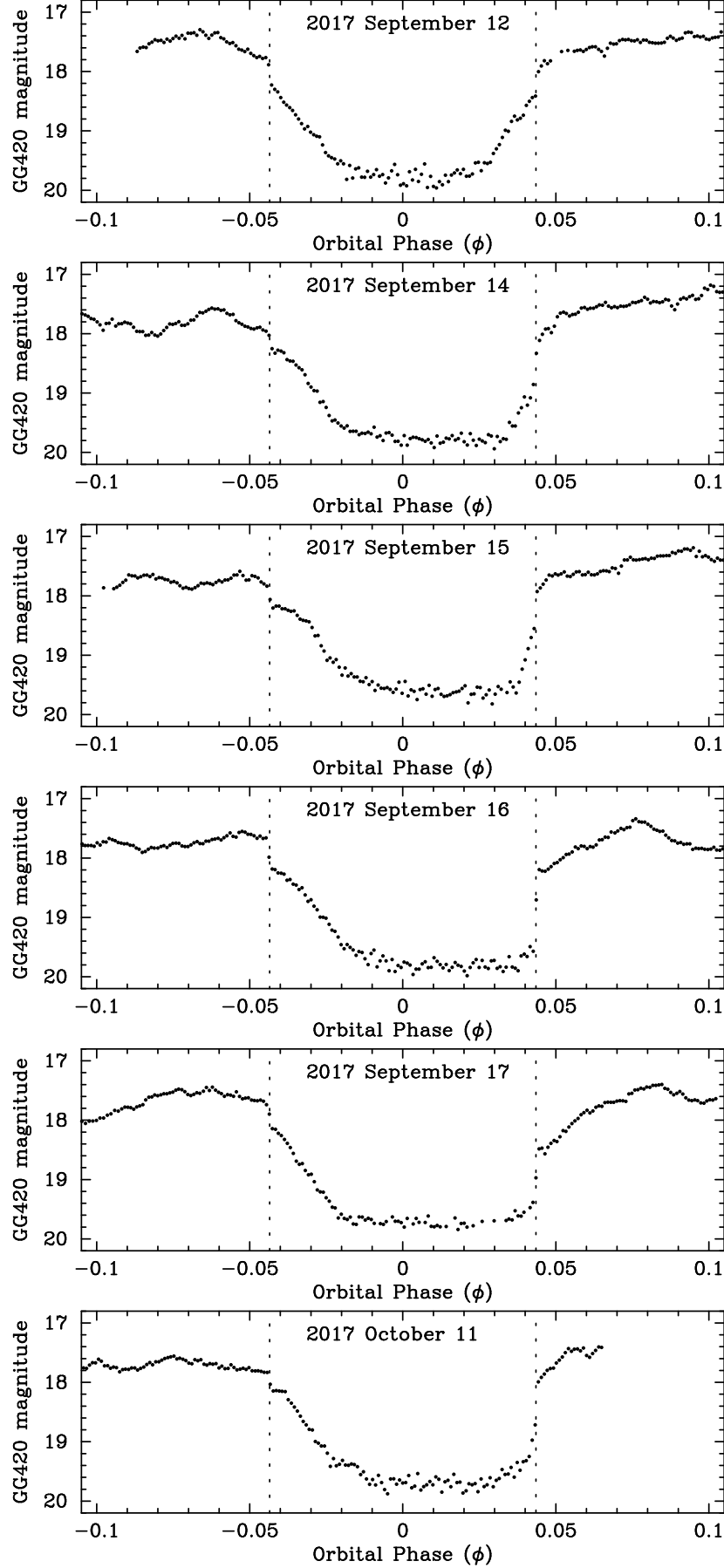


Figure 14. Expanded view of the eclipses of Swift J2116.5+5336. The vertical dotted lines correspond to the ephemerides of WD ingress and egress given in the text. Individual timings are listed in Table 4.

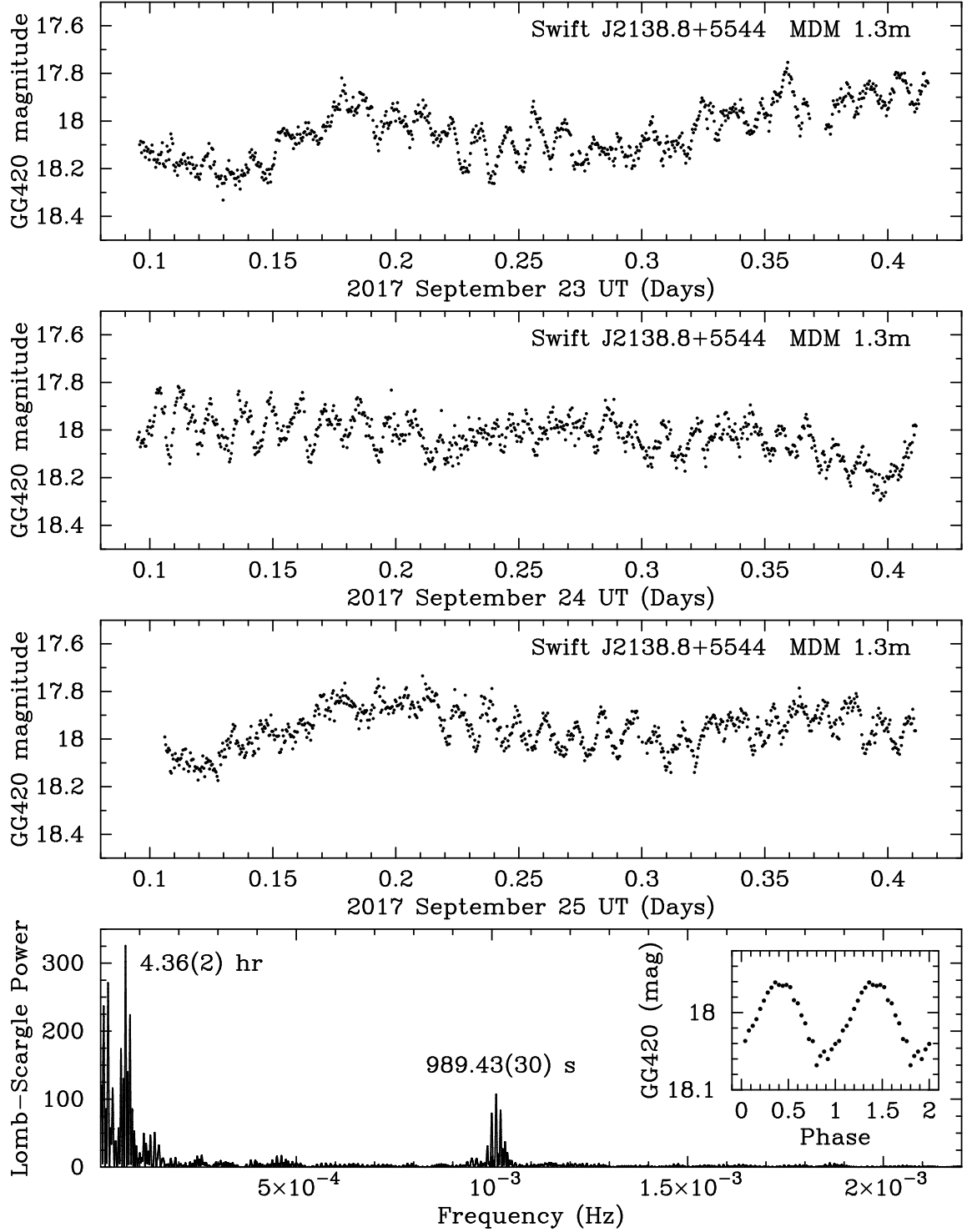


Figure 15. Time-series photometry of Swift J2138.8+5544. Individual exposures are 30 s. The inset shows the light curve folded at $P = 989.43$ s.

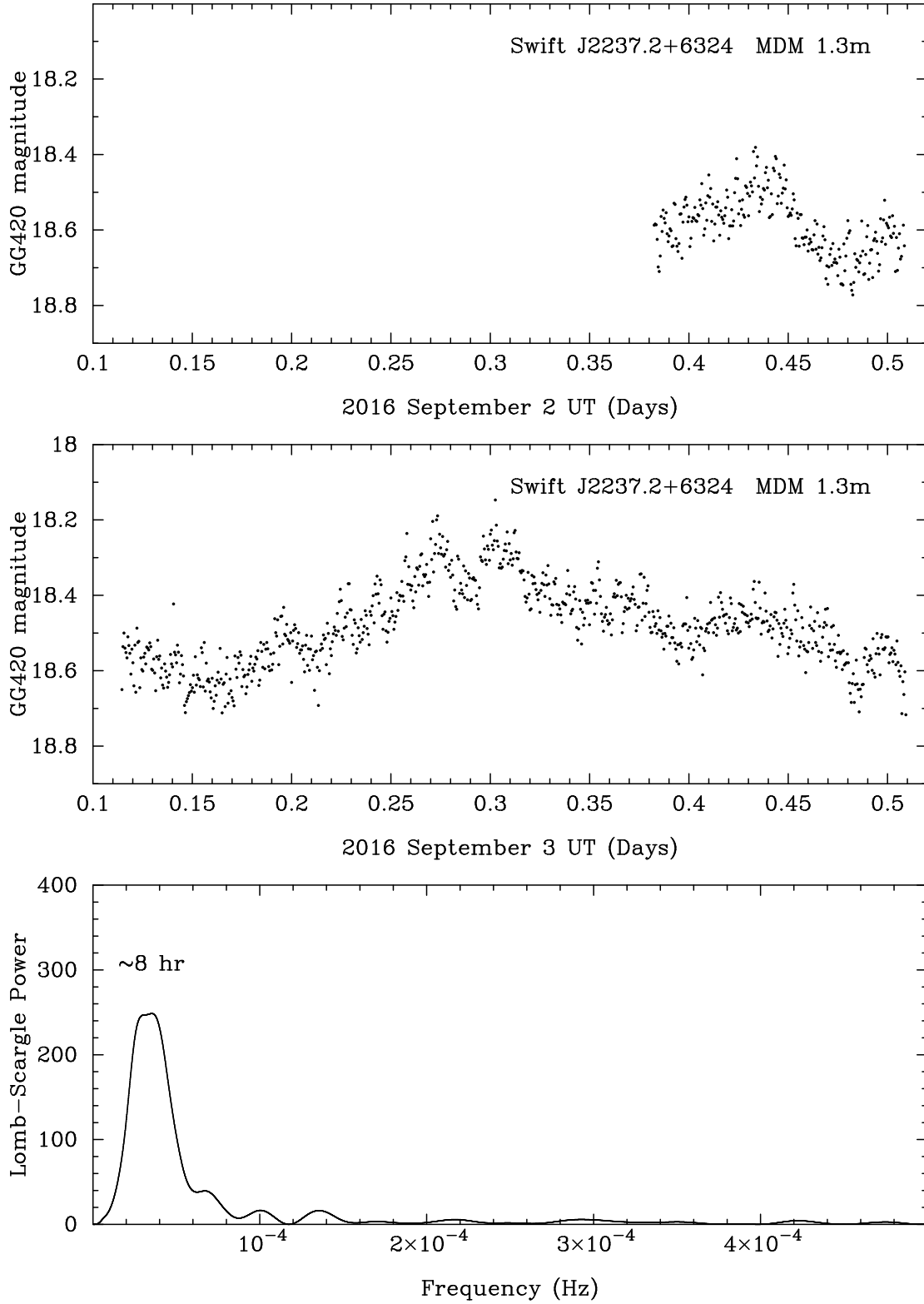


Figure 16. Time-series photometry of Swift J2237.2+6324. Individual exposures are 40 s. The power spectrum of the September 3 data has a peak at ~ 8 hr, approximately the length of the observation.

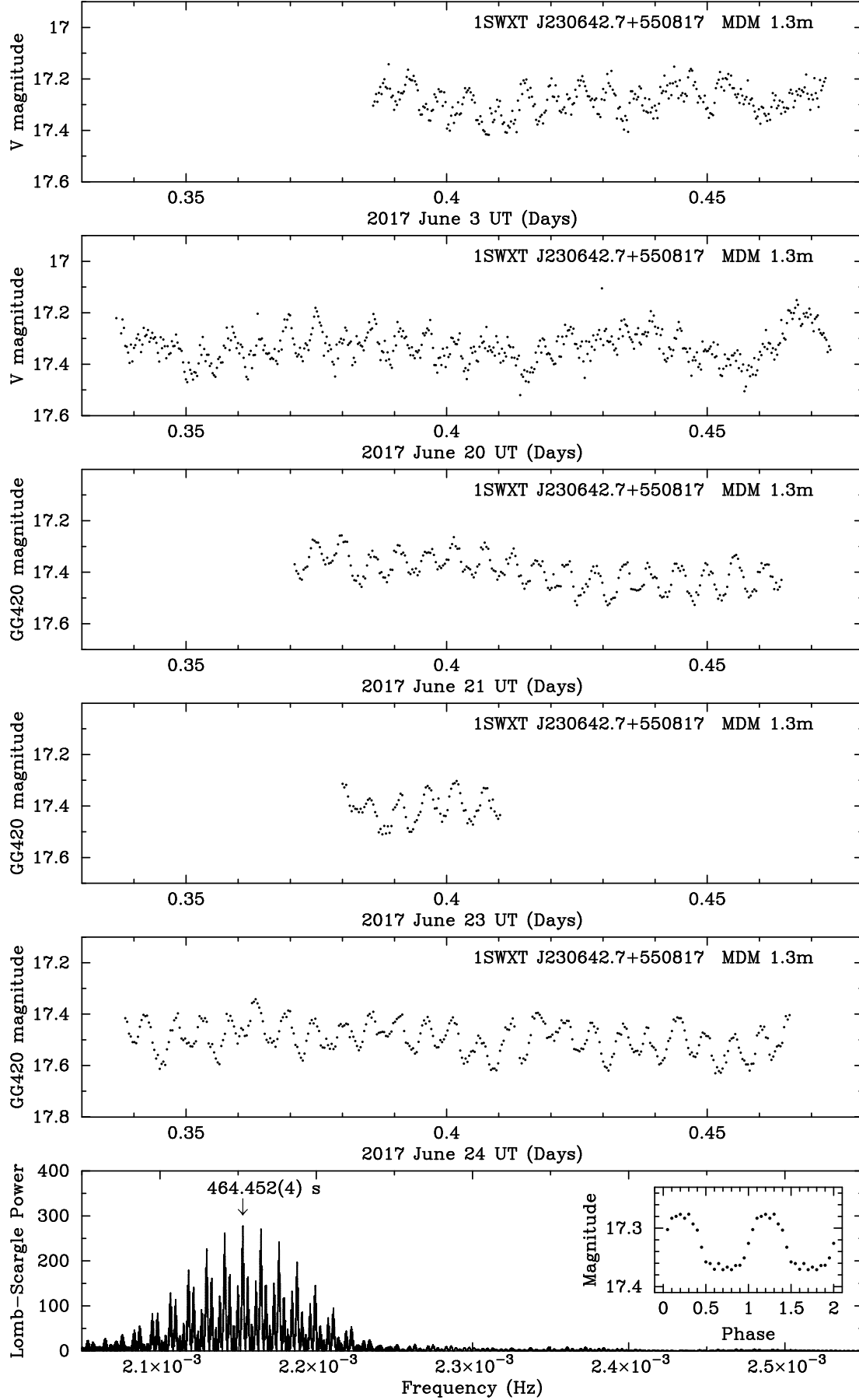


Figure 17. Time-series photometry of 1SWXRT J230642.7+550817. Individual exposures are 20 s in the V filter and 30 s in GG420. The inset shows the light curve folded at $P = 464.452$ s.